HHS Public Access

Author manuscript

Transl Res. Author manuscript; available in PMC 2024 September 11.

Published in final edited form as:

Transl Res. 2023 October ; 260: 17–31. doi:10.1016/j.trsl.2023.05.002.

Diet-induced obesity augments ischemic myopathy and functional decline in a murine model of peripheral artery disease

Emma Fletcher[a], **Dimitrios Miserlis**[b], **Kristina Sorokolet**[a], **Dylan Wilburn**[c], **Cassandra Bradley**[a], **Evlampia Papoutsi**[a], **Trevor Wilkinson**[a], **Andrew Ring**[a], **Lucas Ferrer**[b], **Gleb Haynatzki**[d], **Robert S. Smith**[e], **William T Bohannon**[e], **Panagiotis Koutakis**[a,*]

[a]Department of Biology, Baylor University, Waco, Texas

[b]Department of Surgery, University of Texas at Austin Dell Medical School, Austin, Texas

[c]Department of Health, Human Performance and Recreation, Baylor University, Waco, Texas

[d]Department of Biostatistics, University of Nebraska Medical Center, Omaha, Nebraska

[e]Department of Surgery, Baylor Scott & White Medical Center, Temple, Texas

Abstract

Peripheral artery disease (PAD) causes an ischemic myopathy contributing to patient disability and mortality. Most preclinical models to date use young, healthy rodents with limited translatability to human disease. Although PAD incidence increases with age, and obesity is a common comorbidity, the pathophysiologic association between these risk factors and PAD myopathy is unknown. Using our murine model of PAD, we sought to elucidate the combined effect of age, diet-induced obesity and chronic hindlimb ischemia (HLI) on (1) mobility, (2) muscle contractility, and markers of muscle (3) mitochondrial content and function, (4) oxidative stress and inflammation, (5) proteolysis, and (6) cytoskeletal damage and fibrosis. Following 16-weeks of high-fat, high-sucrose, or low-fat, low-sucrose feeding, HLI was induced in 18-month-old C57BL/6J mice via the surgical ligation of the left femoral artery at 2 locations. Animals were euthanized 4-weeks post-ligation. Results indicate mice with and without obesity shared certain myopathic changes in response to chronic HLI, including impaired muscle contractility, altered mitochondrial electron transport chain complex content and function, and compromised antioxidant defense mechanisms. However, the extent of mitochondrial dysfunction and oxidative stress was significantly greater in obese ischemic muscle compared to non-obese ischemic muscle. Moreover, functional impediments, such as delayed post-surgical recovery of limb function and reduced 6-minute walking distance, as well as accelerated intramuscular protein breakdown, inflammation, cytoskeletal damage, and fibrosis were only evident in mice with obesity. As these features are consistent with human PAD myopathy, our model could be a valuable tool to test new therapeutics.

*Reprint requests: Panagiotis Koutakis, Associate Professor, Department of Biology, Baylor University, B.207 Baylor Science Building, One Bear Place #97388, Waco, TX 76798-7388. panagiotis_koutakis@baylor.edu (P. Koutakis).

Conflicts of Interest: The authors have no competing interests.

Supplementary materials

Supplementary material associated with this article can be found in the online version at doi:10.1016/j.trsl.2023.05.002.

Keywords

peripheral artery disease; ischemic myopathy; Obesity; Age; mitochondriopathy

Introduction

Peripheral artery disease (PAD) is a manifestation of atherosclerosis characterized by progressive narrowing and occlusion of the arteries supplying the lower extremities and affects over 14 million in the U.S. and 236 million people worldwide.[1,2] Symptoms of PAD range in severity from the more common presentation, intermittent claudication (IC) - leg pain elicited with mild exertion and relieved by rest, to critical limb ischemia (CLI) associated with chronic ischemic foot pain at rest, non-healing ulcers or gangrene.[3–6] Although IC and CLI were traditionally considered a product of reduced blood flow,[7,8] altered hemodynamics alone does not fully explain the impaired leg function noted in PAD patients.[3,8–11] Emerging evidence suggests the functional impediments with PAD also result from a myopathy affecting the lower extremity muscles subjected to ischemia and reperfusion.[8,12–16] This loss of viable skeletal muscle in the lower extremities is not only associated with impaired muscle function and limited mobility, but also reduces quality of life, and escalates patient morbidity and mortality.[1,8,12–15,17–19]

The etiological factors mediating the onset of this PAD-associated myopathy are complex but appear to include mitochondrial dysfunction, heightened inflammation, and oxidative stress.[5,9,12,15,16,19–26] However, results from preclinical interventions specifically targeting mitochondria, inflammation and/or oxidative stress show inconsistent efficacy,[19] and agents that have shown promise in animals, often have limited therapeutic success in human randomized trials.[1,27] Taken together, these data suggest the mechanisms underlying PAD myopathy are still not fully understood, methodologies currently employed to model PAD in animals are too variable to yield consistent results, and/or pre-existing animal models have limited translatability to human PAD patients.[19,27]

Although animal models are invaluable for exploring molecular pathways involved in disease development, much of our knowledge to date stems from studies of acute hindlimb ischemia utilizing young, healthy rodents.[19,27–29] While these prior investigations provide insight into the pathophysiology of PAD myopathy, prospective data in humans show that age is an important risk factor for disease development.[30] Indeed, PAD primarily affects those over the age of 40 years, with an estimated 12–20% of the general population developing PAD by age 65 years.[2,5] Consequently, preclinical models with young rodents may not fully replicate the chronic nature of human PAD.[27,29] Moreover, the few existing studies using aged mice have exclusively focused on simulating the severe, acute muscle damage and necrosis noted in CLI,[31,32] which only occurs in approximately 11% of PAD patients.[6] Considering IC has a comparatively higher prevalence, there is much need for a more representative animal model to investigate, and gain a better understanding of, the earlier/less severe stages of PAD myopathy.

The inclusion of comorbid conditions, usually absent in animal models,[27,29,33] would also enhance research translatability. Of the various comorbidities, recent evidence suggests an

important link between obesity and PAD.[30,34,35] Obese individuals with PAD also show a greater loss of calf muscle mass and functional decline than those of a normal body weight.[36] However, the pathophysiologic basis of this association is currently unknown. As the incidence of both obesity and PAD increases with age,[2,5,37] determining the pathological features of PAD myopathy when these risk factors are combined, is crucial for the future development of more efficacious treatment modalities.

In a move toward greater translatability, we herein describe our novel murine model of obese PAD myopathy in aged C57BL/6J mice. The current investigation sought to elucidate the combined effect of age, diet-induced obesity and chronic hindlimb ischemia (HLI) on lower extremity muscle function and pathology. Specifically, the impact of these risk factors on (1) mobility (6-minute walking distance), (2) muscle contractility, as well as markers of (3) mitochondrial content and function, (4) muscle oxidative stress and inflammation, (5) muscle proteolysis (via calpain1, 20S and 26S proteasomes, autophagy, and caspase 3), and (6) muscle cytoskeletal damage (desmin protein abundance) and fibrosis were assessed. We hypothesized muscle contractility, ambulatory ability and mitochondrial function would be impaired, however, muscle protein breakdown, oxidative stress, inflammation, damage, and fibrosis would be increased, in high-fat fed mice with chronic HLI.

Materials and methods

Animals

Fourteen-month-old male and female C57BL/6J mice (n = 12 males, 12 females) (Jackson Laboratories, Bar Harbor, ME) were housed and treated in the Animal Research Facility (ARF) at Baylor University on a 12:12 hours light-dark cycle with access to food and water ad libitum.

Ethics statement

Animal care and procedures were in accordance with the Guide for the Care and Use of Laboratory Animals[38] and approved by the Institutional Animal Care and Use Committee (IACUC) at Baylor University under protocol number 1827226.

Experimental groups and design

Following acclimation to the ARF, the mice were randomized into 2 diet groups. Half (n = 6 males, 6 females) were fed a high-fat, high-sucrose (HFS) diet consistent with the typical western diet,[39] and the remainder a low-fat, low-sucrose control (LFS) diet. The initial feeding phase of the study occurred over a 16-week duration, after which all mice underwent the surgical ligation of the left femoral artery to induce unilateral HLI. To better replicate the chronic nature of human PAD, the induction of HLI was then followed by a 4-week post-ligation feeding phase where study animals continued with their respective HFS or LFS diets. Two males assigned to the HFS group developed ulcerative dermatitis during the initial feeding phase of the study and required humane euthanasia (final n in HFS group = 4 males, 6 females).

Animal diet and food intake and body mass assessment

Mice were fed a HFS (45% kcal fat, 17% sucrose; D12451), or a LFS (10% kcal fat, 0% sucrose; D12450K) chow diet (Open-Source Diets, New Brunswick, NJ) for 20-weeks (16-weeks pre-, and 4-weeks post-surgical intervention). This timeline is sufficient to cause a significant divergence in body mass between diet groups.[39] Except for fat and sucrose, both diets were matched for overall ingredient content. Food was replaced, and intake measured every second day as previously described.[40,41] Body mass was assessed weekly during the initial feeding phase, daily for 1 week immediately following HLI, and every second day for the remainder of the study. Body mass was monitored more closely during the postoperative period to ensure the mice were appropriately coping with the surgical intervention.[42]

Induction of unilateral HLI

After the initial feeding phase, HLI was induced using established techniques,[43] with slight modifications listed below. All mice underwent the surgical ligation of the left femoral artery at 2 locations. Using size 6−0 prolene, the first constricting ligature was placed at the point where the left femoral vessels emerge below the inguinal ligament (proximal to the lateral circumflex femoral artery branch). The second ligature was placed around the distal femoral artery, proximal to the bifurcation of the saphenous and popliteal branches. The right limb served as an internal control condition. Laser Doppler perfusion imaging (moorLDI2, Moor Instruments, Wilmington, Del) was used to subjectively assess blood flow immediately prior to- and following HLI ligations. All surgical and imaging procedures were performed under gaseous anesthesia (isoflurane, Halocarbon Company, River Edge, NJ), and analgesia (ketoprofen 5 mg/kg) was administered subcutaneously immediately prior to all surgeries.

Postoperative clinical scoring

Postoperative assessments were conducted daily on all mice for the first week following the induction of HLI. Scores were assigned for both limb function and the degree of visible limb ischemia according to the Tarlov scale[44] and the modified mouse limb ischemia scale,[32] respectively. Grading scale criteria are described in detail elsewhere.[32,44]

Ambulatory ability (open field test)

The open field test measures voluntary activity and is thought to closely relate to the 6-minute walk test performed in human PAD patients.[45,46] The animals were placed in an open chamber constructed of clear, nonporous plastic (40 (L) x 40 (W) x 40 (H) cm) with a video camera (Digital Video Camera HDV-604S, Sonida, China) suspended over the chamber on an elevated stand,[45,47] and their movement was recorded for 6 minutes.[48] Total distance travelled (cm) was analyzed from the recordings using markerless locomotion measurements with customized automated python-based (version 3.8.1) computer vision software (version 4.6.0). The mice were tested individually 24 hours prior to euthanasia. For consistency, all tests were performed in the morning at the end of the dark cycle (0600) and the test conditions (room lighting, temperature, noise levels) were identical for all animals.[45,49]

Animal euthanasia and tissue collection

Four weeks after the induction of HLI, mice were euthanized by cervical dislocation while under isoflurane anesthesia. Skeletal muscle from the ligated (ischemic) and contralateral nonischemic limb, as well as gonadal fat pads were harvested. Fat pad mass was used as a proxy for central adiposity and obesity status.[40,41] The muscle groups harvested include: (1) the soleus for ex-vivo muscle contractility measures, (2) the gastrocnemius (GA) for mitochondrial high-resolution respirometry measures, muscle protein turnover and damage-related biochemical analyzes, (3) the quadriceps for mitochondrial enzymatic activity and antioxidant assays, and (4) the adductor muscle group for histology. All muscles were trimmed of attached adipose tissue prior to storage (either snap frozen in liquid nitrogen, and stored at −80°C for later biochemical measurements, fixed in methacarn, or placed in an ice-cold physiological buffer solution or BIOPS preservation solution and immediately transferred to the lab for contractility and mitochondrial respiration measurements, respectively).

Ex-vivo muscle contractility

Contractile force measurements were performed using isolated soleus muscles. Immediately after isolation, the muscles were placed in an ice-cold physiological salt solution buffer (pH 7.4) containing (in mM) 130.0 NaCl, 4.7 KCl, 1.2 KH_2PO_4, 1.6 $CaCl_2$, 14.9 $NaHCO_3$, 1.2 $MgSO_47H_2O$, 0.03 EDTA and 5.5 glucose. The muscles were subsequently mounted between 2 force transducers (via the proximal and distal tendons) in a DMT 820MS organ bath system (DMT, Ann Arbor, Mich) containing the physiological salt solution buffer. Following mounting, the muscles were equilibrated for 5 minutes prior to determining optimal physiological muscle length (average L_o of 1.1 cm) via a series of twitch contractions. Per DMT manufacturer instructions specific for murine soleus muscle, a square-pulse electrical stimulator (Stimulator − CS4) was used to perform tetanic tension and measure isometric contraction at 10Hz, 30Hz, 50Hz, 80Hz, and 100Hz. Real time display and recording of all force measurements were performed on a computer with a data acquisition platform (AD Instruments PowerLab Data Acquisition System and LabChart software, DMT, Ann Arbor, Mich). Absolute force (mN) was normalized to muscle mass and an approximate physiological cross-sectional area (PCSA) to determine muscle specific isometric twitch force (N/cm^2).[50,51] PCSA was calculated using a previously described equation,[50] which accounts for the density of mammalian skeletal muscle (1.06 g/cm^3),[52] as well as the myofiber length/whole muscle length ratio of 0.71 for the mouse soleus muscle.[53]

Real time polymerase chain reaction

Total RNA was isolated from snap frozen GA samples using the Direct-zol RNA Microprep Kit (Zymo Research, Irvine, Calif, R2063). The quantity and quality of RNA was determined using a NanoDrop One spectrophotometer, and RNA was reverse transcribed to cDNA using the iScript Reverse Transcription Supermix for RT-qPCR Kit (Bio-Rad, Hercules, Calif, 1708841). PCR reactions used the following target genes: calpain1, caspase 3, forkhead box (Fox) O1, FoxO3, F-box O protein 32 (Fbxo32), tripartite motif containing 63 (TRIM63), autophagy genes (Atg) 7, 10, and 12, microtubule-associated protein 1 light

chain 3 (LC3) alpha, sequestosome 1 (p62), proteasome beta 5 subunit (PSMB5), and the housekeeping gene beta-2-microglobulin. A list of these genes was provided to Bio-Rad who designed the primer pair sequences, which were all contained on custom 96-well SYBR Green plates (dried in well) and are proprietary to Bio-Rad. All PCR reactions were run on a CFX Opus Real-Time PCR System (Bio-Rad, Hercules, Calif). The quantification cycle (Cq) of target genes was normalized to the reference gene (beta-2-microglobulin), and relative normalized expression was calculated using the 2^(-delta delta Cq) method. All samples were run in triplicate, and results were averaged.

Muscle protein isolation for enzymatic activity plate assays and western blotting

Frozen GA and quadricep muscles were homogenized in ice-cold lysis buffers consisting of 40 mM Tris, pH 7.2, 50 mM NaCl, 2 mM βME, 2 mM ATP, 5 mM $MgCl_2$ for the GA samples, or 50 mM Tris-HCl, 150 mM NaCl, 1% NP-40, 0.25% sodium-deoxycholate, 0.1% SDS, and 1x protease inhibitor cocktail (Sigma Aldrich, Burlington, Mass, P8340) for the quadricep muscles. Immediately following homogenization of the GA samples, the lysate was split and a 1x protease inhibitor cocktail (Sigma Aldrich, Burlington, Mass, P8340) was added to half the sample. A protease inhibitor was not added to the GA samples destined for measuring proteolytic activity, as these inhibitors can alter major targets of interest (the proteasomes). Total protein within the homogenates was determined in duplicate using the Pierce BCA assay and bovine serum albumin as a standard (Thermo Scientific, Rockford, Ill, 23225).

Protein analysis by western immunoblot

Protein samples from GA and quadricep muscle homogenate were mixed with 2x Laemmli sample buffer and 2-mercaptoethanol (Bio-Rad Hercules, Calif, 1610747). Using 4%−20% Criterion TGX Precast Midi Protein Gels (Bio-Rad Laboratories, 5671095), 20 μg of protein per sample was separated using electrophoresis in a Criterion Cell Tank (Bio-Rad Laboratories). Proteins were transferred to 0.2 μm Amersham Hybond P polyvinylidene difluoride (PVDF) transfer membranes (Cytiva, Malborough, Mass, 10600021), and total protein per lane was quantified using Ponceau S staining (Boston BioProducts, Milford, Mass, ST180). The membranes were subsequently de-stained with deionized water, blocked in 5% nonfat milk in TBS-Tween at room temperature for 1 hours, and incubated in primary antibodies overnight at 4°C. Primary antibodies used with GA muscle lysates include the proteasome alpha-7 subunit (PSMA7, 1:1000, GeneTex, Irvine, Calif, 113531), Forkhead box O (FoxO)-1 (1:300, Sigma Aldrich, Burlington, Mass, 001252), FoxO3A (1:150, GeneTex, 100277), LC3 (1:1000, ProteinTech, 14600), p62 (1:1000, ProteinTech, 18420), Calpain1 (1:100, GeneTex, 102340), Cas-pase3 (1:500, GeneTex, 110543), Poly (ADP-ribose) polymerase 1 (PARP1, 1:600, GeneTex, 100573), Toll-like receptor 9 (TLR9, 1:600, GeneTex, 100726), Desmin (1:1000, ProteinTech, 16520), and Connective tissue growth factor (CTGF, 1:375, GeneTex, 124233). The primary antibodies superoxide dismutase (SOD)-1 (1:1000, ProteinTech, 10269), catalase (1:750, ProteinTech, 66765), and OxPhos rodent antibody cocktail (1:150, Invitrogen, 458099) were used to probe membranes containing protein from quadricep muscle lysates. The membranes were then incubated with an appropriate HRP-conjugated secondary antibody (Goat anti-Rabbit IgG (1:10,000) or Goat anti-Mouse IgG (1:10,000), Invitrogen, Waltham, Mass, 31462, 31430, respectively)

and Clarity ECL Substrate (Bio-Rad Laboratories, 1705060) was used to visualize the immunoreaction via the ChemiDoc MP Imaging System (Bio-Rad Laboratories). The band intensity of each target protein was quantified by densitometric analysis using Image Lab software (Version 6.1, Bio-Rad Laboratories) and normalized to the density of all ponceau bands (total protein) within each sample lane. Protein levels of each target were expressed as fold change of the protein relative to the LFS non-ischemic (ie, control) muscle group.

Preparation of permeabilized muscle fiber bundles for mitochondrial respiration measurements

Sections of ischemic and non-ischemic white GA muscle (20−30 mg) were gently teased with sharp forceps in ice-cold BIOPS preservation solution containing 7.23 mM dipotassium egtazic acid (K_2-EGTA), 2.77 mM Ca-EGTA, 20 mM imidazole, 20 mM taurine, 5.7 mM adenosine triphosphate (ATP), 14.3 mM phosphocreatine, 50 mM MES potassium salt (K-MES), and 6.56 mM magnesium chloride hexahydrate ($MgCl_2.6H_2O$) (pH 7.1). Teased fiber bundles were then incubated with 30 μg/mL saponin at 4°C for 30 min with gentle rocking to allow for selective permeabilization of the sarcolemma.[54] Permeabilized fiber bundles were then transferred to a mitochondrial respiration medium containing 105 mM K-MES, 30 mM potassium chloride (KCl), 10 mM potassium dihydrogen phosphate (KH_2PO_4), 5 mM $MgCl_2.6H_2O$, and 0.5 mg/mL BSA, and rinsed by rocking for 15 minute at 4°C.

High-resolution measurement of mitochondrial respiration and hydrogen peroxide (H_2O_2) release

An Oroboros O2k Oxygraph FluoRespirometer (Oroboros Instruments, Innsbruck, Austria) consisting of 2 temperature-controlled chambers, each containing a polarographic oxygen sensor and a custom-fitted fluorometer (O2k-Fluo LED2 module), was used to simultaneously measure mitochondrial oxygen consumption (JO_2) and H_2O_2 emission (JH_2O_2) in saponin-permeabilized muscle fibers. Experiments were performed at 37°C in 2 mL of the respiration buffer described above supplemented with creatine monohydrate (20 mM). Fiber bundles were weighed immediately prior to their placement in each Oroboros chamber (approximately 10 mg wet weight per chamber). A substrate inhibitor titration protocol was performed, whereby 2 mM malate and 10 mM glutamate were added to the chambers to measure Complex I, state 2 respiration. This was followed by the addition of 4 mM ADP, to initiate state 3 (ADP-stimulated) respiration. Next, 10 mM succinate was added to the chambers to stimulate electron flow through Complex II. Rotenone (10 μM) was then used to inhibit Complex I, and 1mM of duroquinol was added to measure Complex III. Finally, we added 5 μM antimycin A to inhibit Complex III. followed by 0.4 mM N,N,N',N'-tetramethyl-p-phenylenediamine (TMPD), and 2 mM ascorbate to prevent TMPD auto-oxidation to measure Complex IV.[16,23,55] All reagents and chemicals were purchased from Sigma Aldrich (St. Louis, MO).

The net rate of mitochondrial JH_2O_2 release per electron transport chain (ETC) complex was measured simultaneously during respirometry experiments using Amplex UltraRed reagent (AmR; 5 μM) (Thermo Scientific, Rockford, Ill, A36006) and horseradish peroxidase (HRP; 1 U/mL) as previously described in detail.[56−58] Briefly, JH_2O_2 was detected fluorometrically by monitoring the accumulation of resorufin at each stage of the substrate inhibitor titration

protocol. Resorufin is the stable fluorescent product of 1:1 oxidation of AmR by H_2O_2 in the presence of HRP (at within-chamber excitation/emission wavelengths of 563/587 nm). Resorufin fluorescence was calibrated to chamber H_2O_2 concentration using freshly prepared H_2O_2 standards (0.1 and 1 μM) stabilized with 10 μM HCl.[57,58] The increase in chamber fluorescence resulting from titrations of known H_2O_2 concentration was used to convert the fluorescence signal to within-chamber H_2O_2 content using Datlab software (Oroboros Instruments, Innsbruck, Austria).[57] Once all measurements were complete, fiber bundles were removed from the chambers and stored at −80°C for later citrate synthase (CS) activity measures. Mitochondrial JO_2 and JH_2O_2 are expressed as picomoles per second, normalized to CS activity (pmols/sec/CS activity).[15]

Citrate synthase activity

A CS Assay Kit (Sigma Aldrich, CS0720) was used to measure CS activity in previously permeabilized skeletal muscle lysates as a measure of mitochondrial content.[15,16] Specifically, CS activity was determined colorimetrically using the substrate 5,5'-Dithiobis-(2-nitrobenzoic acid) (DTNB) (10mM). A reaction mix containing the DTNB substrate, muscle lysate (8 protein), 30 mM acetyl coenzyme A (CoA) and 10 mM oxaloacetic acid (OAA) was prepared for all samples. In the presence of OAA, CS catalyzes the reaction between a thiol group of acetyl CoA and DTNB to produce 5-thio-2-nitrobenzoic acid (TNB). Thus, CS activity was measured by monitoring the change in absorbance (ie, TNB formation) every 10 seconds for 5 minutes (25°C) (Varioskan LUX microplate reader, Waltham, Mass) in 96 well plates. All samples were assayed in duplicate at a wavelength of 412 nm with blank values subtracted and reported as micromole activity per minute per ug muscle protein (umol/min/ug protein) determined using a Pierce BCA assay (Thermo Scientific, Rockford, Ill, 23225).

Mitochondrial ETC complex activity

The enzyme activity of all mitochondrial ETC protein complexes in quadricep muscle lysates was determined spectrophotometrically as detailed elsewhere.[59] In brief, Complex I (NADH/CoQ_1 Oxidoreductase) activity was determined in 50 mM potassium phosphate buffer (Kpi), 0.1% BSA, 1 mM KCN, 5 μg/mL antimycin A, pH 7.4, following the oxidation of NADH (50 μM) at 340 nm (30°C, ε_{340} = 6,220 $M^{-1}cm^{-1}$) every 15 seconds for 3 minutes using 50 μM oxidized coenzyme Q_1 (CoQ_1) as the electron acceptor. Rotenone (2.5 μM) was added to measure rotenone-sensitive NADH/CoQ_1 oxidoreductase activity. Complex II (succinate dehydrogenase) activity was measured in Kpi buffer (50 mM, pH 7.4) in the presence of 10 mM succinate, 6 μg/mL antimycin A and 2.5 μM rotenone. After a 10 minutes incubation (30°C), 100 μM CoQ_1 was added to each sample and the rate of CoQ_1 disappearance was measured at 280 nm (ε_{280} = 12,000 $M^{-1}cm^{-1}$) every 15 seconds for 4 minutes. Complex III (Decylubiquinol-Cytochrome C Reductase) activity was measured in Kpi buffer (25 mM, pH 7.5) supplemented with 0.5 mM KCN, 0.1 mM EDTA, 0.025% Tween 20, and oxidized cytochrome *c* (75 μM, the electron acceptor). After the addition of the electron donor, decylubiquinone (100 μM), the rate of cytochrome *c* reduction was measured every 15 seconds for 2 minutes at 550 nm (37°C, ε_{550} = 18,500 $M^{-1}cm^{-1}$). Complex IV (cytochrome *c* oxidase) was determined in 50 mM Kpi buffer (pH 7.0). The decrease in absorbance at 550 nm (37°C, ε_{550} = 18,500 $M^{-1}cm^{-1}$) was followed every 15

seconds for 2 minutes after the reaction mix was supplemented with 60 μM of reduced cytochrome *c*. Potassium cyanide was added to check for the specificity of complex IV activity. Samples for all ETC assays were run in duplicate with blank values subtracted and normalized to the total protein within the muscle lysate. Activity for each ETC complex is reported as nmol/min/mg.

Measures of intramuscular oxidative stress

Oxidative stress was assessed via between-group comparisons of SOD and catalase protein content and activity, as well as the degree of oxidized protein (carbonyl) accumulation.

SOD activity

The enzymatic activity of SOD within quadricep muscle lysates was measured using a commercially available kit (Sigma Aldrich, Burlington, Mass, CS0009) according to the manufacturer's instructions. Briefly, SOD activity within the samples was determined colorimetrically using the kit-provided water-soluble tetrazolium (WST) chromogenic dye, which interacts with superoxide anions generated after the addition of xanthine oxidase. A reaction mix containing the WST dye, muscle lysate (20 μg) and xanthine oxidase was prepared for all samples. After 30 minutes incubation (25°C), the plate was read at 450 nm (Varioskan LUX microplate reader, Waltham, Mass) against a SOD standard. Measurements were performed in duplicate and SOD activity was expressed as units of activity/mL and normalized to the total protein within the muscle homogenate (U/mL/mg).

Catalase activity

Catalase activity was measured within quadricep muscle lysates using a catalase activity kit (Cayman Chemical, Ann Arbor, Mich, 707002) according to the manufacturer's instructions. The samples were assayed in duplicate at a wavelength of 540 nm (Varioskan LUX microplate reader, Waltham, Mass) against a formaldehyde standard. Blank values were subtracted, and enzymatic activity was normalized to the sample total protein (nmol/min/mg).

Protein carbonyl accumulation

Protein carbonyl concentration within the GA muscle was determined via an ELISA kit (OxiSelect, Cell Biolabs, San Diego, Calif, STA310). The assay was read at 450 nm (Varioskan LUX microplate reader, Waltham, Mass) against a known standard. Measurements were performed in duplicate and normalized to the total protein within the muscle homogenate (nmol/mg).

26S and 20S proteasome activity

Chymotrypsin-like activity was measured fluorometrically using the peptide substrates Suc-LLVY (26S proteasome-specific) or Ac-ANW (specific to the 20S proteasome), both labeled with fluorescent AMC (7-amino-4-methylcoumarin), and AMC as the standard (UBPBio, Aurora, Colo, J4110 and G1120). Gastrocnemius muscle homogenates (1.5 μg) treated with the 26S proteasome-specific inhibitor, epoxomicin (20 μM) (UBPBio, F1400), or MG-132 (20S proteasome inhibitor, 200 μM) (UBP-Bio, F1100) served as the negative

controls. Peptidase activity was measured by monitoring AMC liberation every minute for 20 minutes (37°C) (Varioskan LUX microplate reader, Waltham, Mass) in black, 96-well plates (Thermo Scientific, Rockford, Ill, 1256670). Excitation and emission wavelengths were 360nm and 460nm, respectively. Assays were performed in duplicate, with negative control and blank values subtracted. 26S and 20S chymotrypsin-like activity was determined by comparing fluorescence from inhibitor-treated and untreated samples within the linear range of the kinetic curve, with fluorescence of the standard curve.[41,60] Enzyme activity was normalized to the total proteasome content (PSMA7) within each sample.[41,60,61] Normalized activity measures are presented as nmol AMC liberated per minute per PSMA7 density determined from western immunoblots (nmol/min/PSMA7).

Histological analyzes

Immediately after extraction, adductor muscle samples were fixed in ice-cold methacarn. The muscles were subsequently transferred to ice-cold ethanol (50:50 v/v) 48 hours later, embedded in paraffin, and sectioned to a 4 μm thickness as previously described.[15] Muscle fibrosis (collagen deposition) was visualized via a Masson trichrome staining kit (Thermo Scientific, Rockford, Ill, FIS22110648).

Statistical analysis

Prism statistical software (version 8.3.0, GraphPad) was used to perform all analyzes. Significance was accepted at $P < 0.05$. Change in body mass throughout the study, as well as postoperative limb function clinical score between control and obese mice was assessed via a mixed effect ANOVA with Bonferroni post hoc tests. Two-way ANOVA and post-hoc tests using Tukey correction were used to compare final animal body mass and fat mass in male and female mice with and without diet-induced obesity. An independent samples t-test was used to test for within group sex differences for all other variables. Male and female data was combined in the absence of a statistical sex difference. An independent samples t-test was subsequently used to compare between diet-group ambulatory ability. Two-way ANOVA and post-hoc tests using Tukey correction were used to test for differences in all markers of muscle mitochondrial function, oxidative stress, proteolysis, cytoskeleton damage, fibrosis, peak isometric force, and ambulatory ability. Data are reported as mean ± standard error (SE).

Data availability

The datasets generated and/or analyzed during the current study are available from the corresponding author on reasonable request.

Results

Body mass and visceral fat mass

Body mass did not differ in male (HFS: 41.6 ± 0.7 g vs LFS: 44.8 ± 3.2 g, $P = 0.770$) or female mice (HFS: 38.5 ± 3.0 g vs LFS: 35.5 ± 1.7 g, $P = 0.813$) assigned to the 2 diet groups at study onset, but was significantly greater in HFS-fed males (HFS: 48.8 ± 0.5 g vs LFS: 39.7 ± 2.0 g, $P = 0.0004$) and females (HFS: 42.6 ± 3.0 g vs LFS: 32.3 ± 1.6 g, $P = 0.0375$) within 5 and 6 weeks of feeding, respectively. The significant

between-group divergence in body mass continued for the remaining feeding period ($P < 0.05$) (Supplementary Fig 1A and B). At study completion, HFS-fed males and females gained 139% and 127% of their initial body mass, respectively, and visceral fat mass was significantly greater ($P < 0.0001$) in the HFS group (Supplementary Fig 1C).

Except for body mass, there was no within-diet group sex differences noted for any below-listed study variables of interest. Consequently, data from male and female mice within each experimental group were combined and are reported together.

Postoperative doppler imaging and limb function/clinical score

Immediate postligation doppler imaging confirmed blood flow was reduced distal to the ligatures in the affected limb of all animals (Fig 1A). Daily post-surgical assessments revealed functional deficits (ie, reduced Tarlov scores) in mice fed a HFS diet ($P < 0.0001$), which were not returned to baseline by postoperative day 7 ($P = 0.0024$). Mice fed the LFS diet showed no significant deficits at any stage of the postoperative assessment period ($P > 0.05$) (Fig 1B). No gross changes in hindlimb appearance, as assessed via the modified mouse limb ischemia scale,[32] or swelling were apparent for any animal. Consequently, these scored are not reported.

Ambulatory ability and in vitro muscle contractility

Walking distance was significantly reduced in mice exposed to a chronic HFS diet (HFS: 40.9 ± 1.6 cm vs LFS: 53.0 ± 1.6, $P < 0.0001$) when assessed 4 weeks post-HLI surgery (Fig 1C). Force-frequency contractile measurements in isolated soleus muscles also showed a significant decrease in the peak isometric force produced by the ischemic muscle from HFS-fed mice (29.1 ± 7.7 N/cm^2) when compared to nonischemic muscle from the contralateral limb (85.4 ± 15.4 N/cm^2, $P = 0.0448$) and nonischemic LFS control muscle (98.8 ± 20.6 N/cm^2, $P = 0.0036$). Although the average peak force produced by HFS ischemic muscle was 0.46-fold lower than what was noted for the LFS ischemic muscle (63.9 ± 9.6 N/cm^2), this difference was not statistically significant ($P = 0.3075$) (Fig 1D).

Intramuscular mitochondrial content

Since mitochondrial defects can impair both muscle integrity and function,[8,11–16,22,55,62,63] we next sought to determine whether mitochondrial content and activity were altered by chronic overfeeding and/or ischemia in the muscle of our aged mice. Although we saw no change in overall mitochondrial content (CS activity) between experimental groups ($P = 0.3572$) (Fig 2A), western immunoblotting for the individual ETC complexes revealed differences in protein abundance (Fig 2B–G). When compared to control muscle (nonischemic muscle from LFS-fed mice), the protein content of Complexes I, III, and V ($P < 0.0001$, for all) were significantly reduced in the ischemic muscle of both HFS- and LFS-fed mice. However, the fold change reduction of Complex I protein was greater in HFS versus LFS ischemic muscle ($P = 0.0235$), and reductions in Complex II and IV protein were only evident in ischemic muscle from the obese animals (interaction effect $P = 0.0398$ and $P = 0.0173$, respectively).

Mitochondrial function

Irrespective of animal diet group, the oxygen consumption rate was significantly lower in permeabilized ischemic muscle fibers during Complex I, state 3 (CI.3) respiration ($P = 0.0065$), combined Complex I and II (CI+II) respiration ($P = 0.0277$) and Complex III (CIII) respiration ($P = 0.0004$), when compared to nonischemic muscle (Fig 3). Spectrophotometric assessments of muscle lysates also revealed CI enzymatic activity was significantly reduced in ischemic versus nonischemic muscle ($P < 0.0001$). Moreover, HLI also reduced CIII ($P = 0.0016$) and CIV ($P = 0.0060$) activity, but only in ischemic muscle from obese mice (Fig 4). In contrast, mitochondrial H_2O_2 emission from Complex I, state 2 (CI.2) ($P = 0.0004$), CI.3 ($P < 0.0001$), CI+II ($P = 0.0077$), CII ($P < 0.0001$), and CIII ($P < 0.0001$) was significantly increased in ischemic muscle fibers from both obese and normal weight mice. However, H_2O_2 production by CI.3 and CII was greatest in ischemic muscle from HFS-fed mice ($P = 0.0304$ and $P = 0.0041$, vs LFS ischemic muscle, respectively), and CIV $J_{H_2O_2}$ was only elevated in obese ischemic muscle ($P = 0.0058$) (Fig 5).

Intramuscular oxidative stress and inflammation

Despite the rise in mitochondrial H_2O_2 production, the protein content and enzymatic activity of the antioxidant SOD was reduced in ischemic muscle compared to nonischemic muscle ($P < 0.0001$ for both SOD protein and activity). Although no differences in SOD protein expression were noted between LFS and HFS ischemic muscle ($P = 0.9960$) (Fig 6A and B), SOD activity was significantly lower in the ischemic muscle from obese mice (HFS ischemic: 321.6 ± 14.3 U/mL/mg vs LFS ischemic: 419.8 ± 15.1 U/mL/mg, $P = 0.0159$) (Fig 6C). Similarly, the intramuscular protein content and activity of the antioxidant catalase was 0.5-fold ($P < 0.0001$) and 0.3-fold ($P = 0.0332$) lower in ischemic muscle of chronically HFS-fed mice when compared to the ischemic muscle of their LFS-fed counterparts (Fig 6A, D, and E). Moreover, protein carbonyl accumulation, characteristic of oxidative damage,[64] and muscle inflammation assessed from TLR9-probed immunoblots, was only evident in ischemic obese muscle (protein carbonyls: 1.6 ± 0.4-fold increased ($P = 0.0149$) (Fig 6F), TLR9: 1.7 ± 0.1-fold increased ($P = 0.0086$) vs nonischemic LFS controls (Fig 6A and G).

Muscle protein turnover

Chronic oxidative stress and inflammation can promote skeletal muscle breakdown.[65–67] Consequently, we sought to elucidate whether major proteolytic systems (calpain1, caspase 3, the ubiquitin 26S proteasome (UPS) and 20S proteasome systems, and autophagy) were impacted by diet and ischemia. RT-PCR revealed no major experimental group differences in gene expression for any of our markers of interest ($P > 0.05$, Table 1).

Nevertheless, a main effect of chronic HFS feeding was noted for calpain1 protein content ($P = 0.0003$). Specifically, calpain1 was increased 1.5 ± 0.1-fold in nonischemic, and 2.1 ± 0.2-fold in ischemic GA muscle from HFS-fed mice when compared to LFS nonischemic control muscle ($P = 0.0495$ and $P < 0.0001$ vs control muscle, respectively). Although calpain1 was visibly higher in the ischemic versus the nonischemic obese muscle, differences did not reach statistical significance ($P = 0.0637$). Calpain1 protein was unaltered by ischemia in LFS-fed mice ($P = 0.0873$) (Fig 7A and B).

Similarly, the intramuscular protein content of the apoptotic protease,[68] caspase 3, was only increased by animal obesity ($P < 0.0001$). Although an interaction effect was not observed ($P = 0.4238$), caspase 3 protein was significantly greater in obese ischemic muscle compared to ischemic muscle from LFS-fed mice ($P = 0.0042$). Caspase 3 protein was also visibly higher in ischemic versus nonischemic obese muscle; however, these differences were not statistically significant ($P = 0.1521$) (Fig 7A and C).

Since caspase 3 is known to proteolytically cleave the enzyme PARP-1, and this cleavage is considered a characteristic event of apoptosis,[69] we next assessed for PARP-1 protein fragments (85- and 24-kDa) on immunoblots. Subsequent analyzes revealed the 24-kDa fragment was only increased in ischemic muscle from obese mice (1.8 ± 0.2-fold relative to LFS control muscle, $P = 0.0289$). A main effect of muscle ischemia was noted for the intramuscular content of the 85-kDa fragment ($P = 0.0260$), which was increased 1.2 ± 0.1-fold in LFS ischemic, and 1.3 ± 0.1-fold in HFS ischemic muscle relative to LFS nonischemic control muscle. However, posthoc testing showed the only significant group difference was between obese ischemic muscle and LFS nonischemic control muscle ($P = 0.0262$) (Fig 7A and D).

Next, we assessed for any intramuscular alterations in FoxO1 and FoxO3 protein content; major up-stream regulators of the proteasome and autophagy systems.[70–74] Immunoblots revealed FoxO1 protein was increased by chronic HFS-feeding ($P = 0.0077$) (Fig 7A and E). However, FoxO3 was only significantly increased in the ischemic muscle from mice with diet-induced obesity (2.2 ± 0.3-fold, $P = 0.0068$, increased relative to nonischemic muscle from LFS-fed mice) (Fig 7A and F). Chymotrypsin-like activity of the 26S proteasome was also only increased in the ischemic muscle of HFS-fed mice ($P = 0.0173$) (Fig 7G). However, enzymatic activity of the 20S proteasome was unaffected by diet or ischemia ($P = 0.3206$) (Supplementary Fig 2). Additionally, there were no significant group differences observed for the intramuscular protein content of p62 ($P = 0.1378$) (Supplementary Fig 3A and B) or the ratio of LC3-II:LC3-I protein ($P = 0.9314$) (Supplementary Fig 3A and C) (ie, estimates of autophagy activation[75]).

Evidence of muscle cytoskeletal damage and muscle fibrosis

Damage to the cytoskeleton and muscle fibrosis was quantified as intramuscular desmin and CTGF protein abundance on immunoblots, respectively. Hindlimb ischemia significantly increased desmin, but only in muscle from HFS-fed mice (1.8 ± 0.1-fold increased relative to LFS control muscle, $P = 0.0408$) (Fig 8A and B). Although diet-induced obesity increased CTGF protein in nonischemic (1.5 ± 0.2-fold) and ischemic (2.0 ± 0.1-fold) muscle relative to LFS control muscle ($P < 0.0001$), CTGF accumulation was greatest in the ischemic obese muscle ($P = 0.0110$) (Fig 8A and C). Subjective analyzes of Masson-trichrome stained muscle sections showed a similar pattern of muscle fibrosis to CTGF accumulation (Fig 8D).

Discussion

The present study sought to investigate the combined impact of obesity and chronic HLI on muscle function and pathology in aged mice. Based on the surrounding literature, and to the best of our knowledge, we demonstrate for the first time that our model of chronic

HLI induced an ischemic myopathy in aged mice, which was exacerbated by long-term HFS-feeding. Specifically, our results indicate mice with and without obesity shared certain myopathic changes in response to ischemia, including impaired muscle contractility, altered ETC complex content and function, and compromised antioxidant defense mechanisms. Nevertheless, the extent of mitochondrial pathology, dysfunction and oxidative stress was significantly greater in obese ischemic muscle compared to ischemic muscle from their normal-weight counterparts. Moreover, functional impediments, such as delayed post-surgical recovery of limb function (Tarlov score) and reduced 6-minute walking distance, as well as accelerated intramuscular protein breakdown, inflammation, cytoskeletal damage, and fibrosis were only evident in mice with diet-induced obesity. Features, consistent with human PAD muscle pathology.[8,12–14,18,21,22,62,63,76]

Numerous studies indicate chronic malperfusion of the lower extremities induces an ischemic mitochondriopathy in the skeletal muscle of PAD patients. Mitochondrial alterations commonly reported include ultrastructural defects, DNA damage, reduced respiratory capacity (oxidative phosphorylation), ATP production, and increased oxidative stress.[8,11,12,14,15,22,25,26,62,63,76–78] Consequently, our findings that ischemia reduced mitochondrial ETC complex abundance, enzymatic activity, J_{O_2}, and increased H_2O_2 emission in the ischemic muscle of animals from both diet groups, was unsurprising. The fact obese ischemic muscle experienced a greater loss of ETC protein content and activity and heightened oxidative stress, which involved a larger number of ETC complexes, is likely explained, at least in part, by an oversupply of metabolic fuel to the mitochondria.[55,79]

Research suggests chronic overnutrition with obesity is associated with excess macronutrient availability and delivery to the glycolytic and lipolytic metabolic pathways. The substrate overload to these pathways generates large amounts of the electron donors NADH (nicotinamide adenine dinucleotide dehydrogenase) and $FADH_2$ (1,5-dihydroflavin adenine dinucleotide), subsequently shuttled to the mitochondrial ETC. However, the rate at which the ETC system operates is governed by energy demand, and not substrate supply. Thus, in the absence of increased metabolic demand, the increase in NADH and $FADH_2$ facilitates the donation of electrons to molecular oxygen to form disproportionately high levels of reactive oxygen species (ROS), such as the superoxide anion and H_2O_2.[55,79–81] Transient increases in ROS to moderate/physiologic concentrations are essential for certain cell functions, including, but not limited to, antioxidant gene expression and the maintenance of redox balance. Conversely, ROS cause oxidative tissue injury when production is sustained and cellular concentrations reach supraphysiological levels.[81,82]

Antioxidant defense systems, such as the enzymes SOD and catalase, can protect tissues from ROS-induced damage.[8,14,55,76,77,79,83] The current investigation shows SOD and catalase activity was reduced in ischemic muscle of mice with and without obesity. Considering excessive ROS production can also damage the ETC components,[14,62] an impaired redox balance could explain why ischemic muscle from both animal diet groups experienced a reduction in ETC complex content, activity, and respiration. Nevertheless, the activity of both antioxidants was significantly lower in obese ischemic muscle. Moreover, protein carbonylation, a major hallmark of oxidative damage noted in human PAD myopathy,[8,14,22,63] was only increased in ischemic muscle of HFS-fed mice. Taken together,

these data suggest the antioxidant mechanisms were overwhelmed by the abnormally elevated ROS levels in obese ischemic muscle but were sufficiently active in LFS ischemic muscle to prevent oxidative damage beyond the mitochondrial ETC.

In further support of the above hypothesis, an ischemia-associated increase in TLR9 protein was also only evident in the muscle of obese mice. Toll-like receptor 9 is a pattern recognition receptor expressed by immune and nonimmune cells in response to an intracellular increase in oxidatively damaged mitochondrial DNA (mtDNA).[84–87] Due to the proximity to the ETC, mtDNA is particularly vulnerable to oxidation-induced damage and mutation.[14,85] Moreover, recent evidence shows persistent ROS-associated mitochondrial stress triggers the opening of the mitochondrial permeability transition pore,[76,88,89] and the release of mtDNA into the surrounding cytoplasm.[88] Interaction of TLR9 with oxidized mtDNA, subsequently activates nuclear factor-κB signaling, which increases the expression of pro-inflammatory cytokines.[84,86,87] Although, we did not directly assess for mtDNA damage, previous research shows TLR9 activation, and the initiation of the inflammatory cascade is dependent on the presence of oxidized mtDNA and will not occur when oxidized residues are absent.[87] Consequently, our observation that intramuscular TLR9 content was increased suggests the combination of obesity and HLI triggered mtDNA damage and muscle inflammation, features also evident in human PAD myopathy.[14,24,90–92]

Heightened mitochondrial dysfunction and oxidative stress can also play a central role in upregulating muscle proteolytic systems.[65] First, mitochondria are important regulators of intracellular calcium homeostasis, and dysregulation can lead to apoptosis.[93–95] For instance, the Ryanodine receptor 1 (RyR1) and the ATPase of the sarcoplasmic reticulum (SERCA), vital for intramuscular calcium handling, are highly susceptible to ROS-induced oxidative modification and damage. Thus, when mitochondrial ROS emission is chronically elevated, the subsequent dysfunction of SERCA and the RyR1 raises intracellular calcium concentrations.[95–98] Additionally, the ROS-related increase in outer mitochondrial membrane permeability was previously shown to reduce mitochondrial calcium retention capacity in a rat model of acute hindlimb ischemia.[20,89] The ensuing accumulation of intercellular calcium, together with enhanced oxidative stress can activate the calpain and caspase 3 apoptotic pathways.[95,97,98]

Interestingly, the current investigation found calpain1 and caspase 3 proteins were increased in both the ischemic and non-ischemic muscle of mice fed a HFS diet. Thus, obesity may predispose muscle to apoptosis, even in the absence of a direct ischemic insult. Although non-ischemic obese muscle showed no major alteration in mitochondrial-derived H_2O_2, other sources of ROS exist. For example, obesity is associated with an intramuscular accumulation of excess free fatty acids, which stimulate the de novo synthesis of toxic lipid species such as diacylglycerol and ceramides.[99,100] These lipid intermediaries can trigger ROS production from nicotinamide adenine dinucleotide phosphate oxidase (NOX) enzymes widely expressed in numerous cell types, including adipocytes and muscle.[100,101] Consequently, heightened NOX activity might account for the increase in calpain1 and caspase 3 noted in the nonischemic obese muscle.

However, despite the aforementioned increases, calpain 1 tended to be higher in the ischemic muscle ($P = 0.0637$ vs nonischemic muscle) of HFS-fed mice. Additionally, PARP fragments, cleavage products of caspase 3, were only increased in obese ischemic muscle. Poly(ADP-ribose) polymerase-1 is a nuclear protein involved in DNA repair. During caspase-dependent apoptosis, PARP-1 is cleaved into 24 kDa and 89 kDa fragments, and their appearance is widely regarded as hallmarks of apoptosis in response to massive DNA damage.[102,103] Following cleavage, the 24 kDa fragment irreversibly binds to DNA breaks, preventing additional PARP-1 activation and thus, DNA repair.[102] In contrast, the 89 kDa fragment translocates to the cytoplasm to activate additional apoptotic pathways.[103] As these fragments were only increased in the ischemic muscle of obese mice, we infer ischemia had an additive effect on intramuscular apoptosis in the obese state. However, PARP-1 fragmentation could also signify a protective mechanism against cell necrosis. For instance, although PARP-1 is vital for DNA repair under moderately damaging conditions, pathology can occur if this protein is under-or over-active. Indeed, PARP-1 overactivation can lead to cell death by necrosis through the depletion of its substrate, nicotinamide-adenine dinucleotide, and ultimately cellular ATP.[104] Moreover, a recent study found gastrocnemius muscle PARP-1 abundance was inversely associated with walking performance in patients with PAD.[105] However, since the investigators also found no difference in intramuscular PARP-1 content between PAD and healthy controls, further research is required to determine the full pathological significance of PARP-1 in PAD myopathy.

Aside from apoptosis, the present study showed a significant increase in 26S proteolytic activity, which was exclusive to obese ischemic muscle. In contrast, intramuscular autophagy was unaffected by ischemia or animal diet. Autophagy is a vital quality control mechanism enabling the selective bulk degradation of damaged organelles, including mitochondria, in response to stress.[106] Considering the reduced protein abundance of the mitochondrial ETC complexes, together with an upregulation in mitochondrial ROS emission, intramuscular TLR9 content and apoptotic pathways, the absence of an autophagic response was surprising. Nevertheless, a primary aim of the current investigation was to develop an animal model representing the earlier/less severe stages of PAD myopathy. In support of our model, a recent study found autophagic flux, assessed via the LC3II:LC3I ratio, was increased in the gastrocnemius muscle of patients with moderate to severe disease, but not in patients with mild to moderate disease.[107] Thus, the severity of the mitochondriopathy noted in the ischemic muscle of our animals may not have reached a threshold requiring global mitochondrial degradation, and the breakdown of single mitochondrial proteins likely occurred via other proteolytic pathways.

Several investigations report a link between the ubiquitination and subsequent 26S proteasome-mediated breakdown of outer mitochondrial membrane proteins.[108] However, emerging evidence suggests intra-mitochondrial proteins, including those of the ETC, are also targets of the UPS system.[109] Specifically, Lavie et al.,[109] show protein ubiquitination occurs in numerous mitochondrial compartments, including the inner mitochondrial membrane. Moreover, the turnover of several subunits of the ETC complexes, such as GRIM19 (Complex I), subunit A of succinate dehydrogenase (Complex II), and COX IV (Complex IV), was dependent on the UPS in numerous cell types, including human primary skeletal muscle myoblasts. Additionally, and/or alternatively, intra-mitochondrial

proteins can also be degraded via calpain1.[110] For example, an ischemia-associated activation of mitochondrial calpain1 in cardiac muscle was previously shown to mediate the cleavage of complex I and complex V ETC subunits (subunits NDUFS7 and ATP5A1, respectively).[110–112] Whether the same occurs in ischemic skeletal muscle remains to be determined. Nevertheless, these findings suggest the combined upregulation of calpain1 and 26S catalytic activity could, at least partially, account for the heightened reduction in ETC complex abundance noted in the ischemic muscle of obese mice in our study.

Aside from their impact on mitochondria, accelerated calpain1, caspase 3, and UPS activity are all long known to cause an imbalance between muscle protein synthesis and breakdown in situations of oxidative stress. Chronic overactivation of these pathways can ultimately result in muscle atrophy and impaired muscle function.[65,97,113] Briefly, caspase 3 promotes the degradation of the contractile actomyosin complexes into smaller fragments for subsequent UPS breakdown.[65,68] Recent evidence also indicates the oxidation of actin and myosin increases their susceptibility for calpain degradation.[97] However, calpain 1 primarily facilitates the cleavage of cytoskeletal proteins responsible for maintaining myofibrillar structural integrity. Such cleavage promotes myofibril protein release for further breakdown via other pathways. Cytoskeletal targets of calpain1 include desmin, alpha-actinin, tropomyosin, nebulin, troponin, and titin.[97] Desmin is responsible for attaching the z-disc to the sarcolemma and considered vital for maintaining the structure, shape, and function of the myofiber and affiliated organelles, especially the mitochondria. In the current investigation, we demonstrate desmin protein abundance increased in the ischemic muscle of obese mice, an acknowledged manifestation of cytoskeletal damage.[114] Although insufficient sample prevented further histochemical analyzes of intramuscular desmin in the current study, desmin disorganization and accumulation was previously correlated with altered gastrocnemius myofiber morphology, fibrosis, mitochondrial dysfunction, as well as reduced isometric strength and mobility in patients with PAD.[114] While future work is required to confirm whether a change in desmin protein abundance, as noted in the obese ischemic muscle of the current investigation, corresponds with histologic disturbances to desmin, the consistent findings between the mice of the present study and human PAD patients, further supports the translatability of our murine model.

Of note, oxidative damage in PAD muscle is not limited to the myofiber compartment, but can also occur throughout the extracellular matrix (ECM) to contribute toward muscle fibrosis.[12] Considering an increase in desmin is also associated with intramuscular fibrosis,[12,114] we next sought to determine whether CTGF, a strong profibrotic growth factor, was altered by chronic obesity and/or ischemia in aged mice. We found CTGF was significantly increased, but only in ischemic muscle of obese mice. As CTGF is known to promote excessive ECM accumulation in hypoxic conditions,[115–117] our findings suggest the combination of age and obesity promotes intramuscular fibrosis in mice with chronic HLI. Subjective analyzes of Masson's Trichrome-stained muscle sections further confirmed the expansion of the ECM in the ischemic muscle of HFS-fed animals. These findings contrast with other models of HLI using C57BL/6 mice, which suggest ischemia-induced muscle fibrosis is only reproducible in Balb/c animals.[118] However, these prior studies used relatively young (12−14-week-old) mice fed standard rodent chow. Although direct between-study comparisons can thus not be made, the inconsistencies emphasize the

importance of considering animal age and comorbidities when designing models of human PAD.

The cytoskeleton and ECM are not only important for muscle structural support and integrity. For instance, the cytoskeleton, desmin in particular, is vital for transmitting forces generated through sarcomere contraction to the ECM.[114] In turn, the ECM stores and transmits these forces to tendons and bones.[117] Consequently, cytoskeletal damage and fibrosis, together with mitochondrial dysfunction, were all likely contributors to the functional impediments (reduced ambulatory ability and muscle contractility) noted in the obese animals of the current investigation. Although there were no significant differences in peak isometric force in the ischemic muscle of mice with and without obesity, force tended to be lower in the HFS group. As we noted a relatively large variability in the contractile data, a larger sample size would have likely yielded significant results. However, further clarification is required.

This study is not without limitations. First, although we saw no statistical differences between male and female mice in our primary outcomes of interest, there is the risk that sex differences were masked by the relatively small sample size. Considering there is evidence to suggest a sexual dimorphism exists in the arterial pathophysiology underlying PAD,[119] further work is required to confirm our myopathic findings in males and females. In addition, although we clearly show obese mice experienced greater mitochondriopathy, oxidative stress, muscle protein breakdown and impaired muscle function in response to HLI, cause and effect relationships cannot be established due to the descriptive nature of these observations. Lastly, as we relied on between-group comparisons of protein expression from western immunoblots as a proxy for muscle degradative pathways such as those involved in DNA damage, as well as markers of cytoskeletal damage, future work is required to confirm our results.

Despite these limitations, the present study is the first to perform such a comprehensive assessment of myopathic and functional alterations in response to chronic HLI. Moreover, the pathological features observed in the ischemic muscle of our aged obese mice are consistent with those noted in human patients with mild to moderate-stage PAD.[8,12–14,18,21,22,62,63,76] Consequently, the murine model described herein could be a valuable tool to evaluate new therapeutic modalities which could subsequently be translated to clinical practice.

Supplementary Material

Refer to Web version on PubMed Central for supplementary material.

Acknowledgments

This work was supported by the National Institute on Aging of the National Institutes of Health under Award Numbers R01AG064420 (P.K.). The content is solely the responsibility of the authors and does not necessarily represent the official views of the National Institutes of Health. Additionally, the study was supported by the San Antonio Medical Foundation (P.K., D.M.).

The authors would like to thank all the Baylor University ARF personnel that supported this study. The authors have read the journal's policy on disclosure of potential conflicts of interest.All the authors have read and approved the manuscript.

Abbreviations:

ARF	animal research facility
Atg7	autophagy gene 7
Atg10	autophagy gene 10
Atg12	autophagy gene12
CI.2	mitochondrial Complex I, state 2 respiration
CI.3	mitochondrial Complex I, state 3 respiration
CI+II	combined Complex I and II respiration
CIII	mitochondrial Complex III
CIV	mitochondrial Complex IV
CV	mitochondrial Complex V
CLI	critical limb ischemia
CS	citrate synthase
CTGF	connective tissue growth factor
ECM	extracellular matrix
ETC	electron transport chain
$FADH_2$	1,5-dihydroflavin adenine dinucleotide
Fbxo32	F-box O protein 32
FoxO1	forkhead box O1
FoxO3	forkhead box O3
GA	gastrocnemius
HFS	high-fat, high-sucrose
HLI	hindlimb ischemia
IACUC	Institutional Animal Care and Use Committee
IC	Intermittent claudication
Isch	ischemic
***J*H_2O_2**	mitochondrial hydrogen peroxide emission

JO_2	mitochondrial oxygen consumption
LC3	microtubule-associated protein 1 light chain 3
LC3-II:LC3-I	microtubule-associated protein 1 light chain 3 isoform two-to-one ratio
LFS	low-fat, low-sucrose
mtDNA	mitochondrial DNA
NADH	nicotinamide adenine dinucleotide dehydrogenase
NI	non-ischemic
NOX	nicotinamide adenine dinucleotide phosphate oxidase
p62	sequestosome 1
PAD	Peripheral artery disease
PARP-1	Poly (ADP-ribose) polymerase 1
PCSA	physiological cross-sectional area
PSMA7	proteasome alpha 7 subunit
PSMB5	proteasome beta 5 subunit
ROS	reactive oxygen species
RyR1	Ryanodine receptor 1
SERCA	sarcoplasmic reticulum
SOD1	superoxide dismutase 1
TLR9	Toll-like receptor 9
TRIM63	tripartite motif containing 63
UPS	ubiquitin 26S proteasome

References

1. Annex BH, Cooke JP. New directions in therapeutic angiogenesis and arteriogenesis in peripheral arterial disease. Circ Res 2021;128:1944–57. [PubMed: 34110899]
2. Song P, Rudan D, Zhu Y, et al. Global, regional, and national prevalence and risk factors for peripheral artery disease in 2015: an updated systematic review and analysis. Lancet Glob Health 2019;7:e1020–30. [PubMed: 31303293]
3. Behroozian A, Beckman JA. Microvascular disease increases amputation in patients with peripheral artery disease. Arterioscler Thromb Vasc Biol 2020;40:534–40. [PubMed: 32075418]
4. Ismaeel A, Papoutsi E, Miserlis D, et al. The nitric oxide system in peripheral artery disease: connection with oxidative stress and biopterins. Antioxidants (Basel) 2020;9:590–606. [PubMed: 32640613]

5. Paradis S, Charles AL, Meyer A, et al. Chronology of mitochondrial and cellular events during skeletal muscle ischemia-reperfusion. Am J Physiol Cell Physiol 2016;310:C968–82. [PubMed: 27076618]
6. Anantha-Narayanan M, Doshi RP, Patel K, et al. Contemporary trends in hospital admissions and outcomes in patients with critical limb ischemia: an analysis from the National Inpatient Sample Database. Circ Cardiovasc Qual Outcomes 2021;14:e007539. [PubMed: 33541110]
7. Koutakis P, Ismaeel A, Farmer P, et al. Oxidative stress and antioxidant treatment in patients with peripheral artery disease. Physiol Rep 2018;6:e13650. [PubMed: 29611350]
8. Pipinos II, Judge AR, Selsby JT, et al. The myopathy of peripheral arterial occlusive disease: part 1. Functional and histomorphological changes and evidence for mitochondrial dysfunction. Vasc Endovascular Surg 2007;41:481–9. [PubMed: 18166628]
9. Pellegrin M, Bouzourene K, Poitry-Yamate C, et al. Experimental peripheral arterial disease: new insights into muscle glucose uptake, macrophage, and T-cell polarization during early and late stages. Physiol Rep 2014;2:e00234. [PubMed: 24744903]
10. Poredos P, Jezovnik MK. Why to evaluate the functional capacity in PAD patients? Vasa 2020;49:275–80. [PubMed: 32019475]
11. Ryan TE, Schmidt CA, Green TD, et al. Mitochondrial regulation of the muscle micro-environment in critical limb ischemia. Front Physiol 2015;6:336. [PubMed: 26635622]
12. Weiss DJ, Casale GP, Koutakis P, et al. Oxidative damage and myofiber degeneration in the gastrocnemius of patients with peripheral arterial disease. J Transl Med 2013;11:230. [PubMed: 24067235]
13. Koutakis P, Weiss DJ, Miserlis D, et al. Oxidative damage in the gastrocnemius of patients with peripheral artery disease is myofiber type selective. Redox Biol 2014;2:921–8. [PubMed: 25180168]
14. Pipinos II, Judge AR, Selsby JT, et al. The myopathy of peripheral arterial occlusive disease: part 2. Oxidative stress, neuropathy, and shift in muscle fiber type. Vasc Endovascular Surg 2008;42:101–12. [PubMed: 18390972]
15. Pipinos II, Swanson SA, Zhu Z, et al. Chronically ischemic mouse skeletal muscle exhibits myopathy in association with mitochondrial dysfunction and oxidative damage. Am J Physiol Regul, Integr Comp Physiol 2008;295:R290–6. [PubMed: 18480238]
16. Ryan TE, Yamaguchi DJ, Schmidt CA, et al. Extensive skeletal muscle cell mitochondriopathy distinguishes critical limb ischemia patients from claudicants. JCI Insight 2018;3:e123235–52. [PubMed: 30385731]
17. Leutzinger TJ, Koutakis P, Fuglestad MA, et al. Peripheral artery disease affects the function of the legs of claudicating patients in a diffuse manner irrespective of the segment of the arterial tree primarily involved. PLoS One 2022;17:e0264598. [PubMed: 35830421]
18. Thompson JR, Swanson SA, Haynatzki G, et al. Protein concentration and mitochondrial content in the gastrocnemius predicts mortality rates in patients with peripheral arterial disease. Ann Surg 2015;261:605–10. [PubMed: 24670845]
19. Pizzimenti M, Meyer A, Charles AL, et al. Sarcopenia and peripheral arterial disease: a systematic review. J Cachexia Sarcopenia Muscle 2020;11:866–86. [PubMed: 32648665]
20. Paradis S, Charles AL, Georg I, et al. Aging exacerbates ischemia-reperfusion-induced mitochondrial respiration impairment in skeletal muscle. Antioxidants (Basel) 2019;8:168–79. [PubMed: 31181751]
21. Cluff K, Miserlis D, Naganathan GK, et al. Morphometric analysis of gastrocnemius muscle biopsies from patients with peripheral arterial disease: objective grading of muscle degeneration. Am J Physiol Regul Integr Comp Physiol 2013;305:R291–9. [PubMed: 23720135]
22. Pipinos II, Sharov VG, Shepard AD, et al. Abnormal mitochondrial respiration in skeletal muscle in patients with peripheral arterial disease. J Vasc Surg 2003;38:827–32. [PubMed: 14560237]
23. Ismaeel A, Fletcher E, Miserlis D, et al. Skeletal muscle MiR-210 expression is associated with mitochondrial function in peripheral artery disease patients. Transl Res 2022;246:66–77. [PubMed: 35288364]

24. Casale GP, Thompson JR, Carpenter LC, et al. Cytokine signature of inflammation mediated by autoreactive Th-cells, in calf muscle of claudicating patients with Fontaine stage II peripheral artery disease. Transl Res 2021;228:94–108. [PubMed: 32835907]
25. Brass EP. Skeletal muscle metabolism as a target for drug therapy in peripheral arterial disease. Vasc Med 1996;1:55–9. [PubMed: 9546916]
26. Brass EP, Hiatt WR. Acquired skeletal muscle metabolic myopathy in atherosclerotic peripheral arterial disease. Vasc Med 2000;5:55–9. [PubMed: 10737157]
27. Krishna SM, Omer SM, Golledge J. Evaluation of the clinical relevance and limitations of current pre-clinical models of peripheral artery disease. Clin Sci (Lond) 2016;130:127–50. [PubMed: 26678170]
28. Padgett ME, McCord TJ, McClung JM, Kontos CD. Methods for acute and subacute murine hindlimb ischemia. J Vis Exp 2016;112:e54166–74.
29. Aref Z, de Vries MR, Quax PHA. Variations in surgical procedures for inducing hind limb ischemia in mice and the impact of these variations on neovascularization assessment. Int J Mol Sci 2019;20:3704–18. [PubMed: 31362356]
30. Hicks CW, Yang C, Ndumele CE, et al. Associations of obesity with incident hospitalization related to peripheral artery disease and critical limb ischemia in the ARIC study. J Am Heart Assoc 2018;7:e008644. [PubMed: 30369315]
31. Rivard A, Fabre JE, Silver M, et al. Age-dependent impairment of angiogenesis. Circulation 1999;99:111–20. [PubMed: 9884387]
32. Westvik TS, Fitzgerald TN, Muto A, et al. Limb ischemia after iliac ligation in aged mice stimulates angiogenesis without arteriogenesis. J Vasc Surg 2009;49:464–73. [PubMed: 19028053]
33. Waters RE, Terjung RL, Peters KG, Annex BH. Preclinical models of human peripheral arterial occlusive disease: implications for investigation of therapeutic agents. J Appl Physiol (1985) 2004;97:773–80. [PubMed: 15107408]
34. Heffron SP, Dwivedi A, Rockman CB, et al. Body mass index and peripheral artery disease. Atherosclerosis 2020;292:31–6. [PubMed: 31739257]
35. Huang Y, Xu M, Xie L, et al. Obesity and peripheral arterial disease: a Mendelian randomization analysis. Atherosclerosis 2016;247:218–24. [PubMed: 26945778]
36. Raval Z, Liu K, Tian L, et al. Higher body mass index is associated with more adverse changes in calf muscle characteristics in peripheral arterial disease. J Vasc Surg 2012;55:1015–24. [PubMed: 22365177]
37. Zamboni M, Mazzali G. Obesity in the elderly: an emerging health issue. Int J Obes (Lond) 2012;36:1151–2. [PubMed: 22964828]
38. National Research Council (U.S.) IfLARUS. Guide for the care and use of laboratory animals. 8th ed. Washington (DC): National Academies Press; 2011.
39. Wang CY, Liao JK. A mouse model of diet-induced obesity and insulin resistance. Methods Mol Biol 2012;821:421–33. [PubMed: 22125082]
40. Fletcher E, Gordon PM. Obesity-induced alterations to the immunoproteasome: a potential link to intramuscular lipotoxicity. Appl Physiol Nutr Metab 2021;46:485–93. [PubMed: 33186056]
41. Fletcher E, Wiggs M, Greathouse KL, Morgan G, Gordon PM. Impaired proteostasis in obese skeletal muscle relates to altered immunoproteasome activity. Appl Physiol Nutr Metab 2022;47:555–64. [PubMed: 35148206]
42. Talbot SR, Biernot S, Bleich A, et al. Defining body-weight reduction as a humane endpoint: a critical appraisal. Lab Anim 2020;54:99–110. [PubMed: 31665969]
43. Niiyama H, Huang NF, Rollins MD, Cooke JP. Murine model of hindlimb ischemia. J Vis Exp 2009;23:e1035–9.
44. Tarlov IM. Spinal cord compression studies. III. Time limits for recovery after gradual compression in dogs. AMA Arch Neurol Psychiatry 1954;71:588–97. [PubMed: 13157688]
45. Phie J, Krishna SM, Kinobe R, et al. Effects of quercetin on exercise performance, physical activity and blood supply in a novel model of sustained hind-limb ischaemia. BJS Open 2021;5:zraa059–66.

46. Krishna SM, Omer SM, Li J, Morton SK, Jose RJ, Golledge J. Development of a two-stage limb ischemia model to better simulate human peripheral artery disease. Sci Rep 2020;10:3449. [PubMed: 32103073]
47. Seibenhener ML, Wooten MC. Use of the Open Field Maze to measure locomotor and anxiety-like behavior in mice. J Vis Exp 2015: e52434. [PubMed: 25742564]
48. Gibbs EM, Crosbie-Watson RH. A simple and low-cost assay for measuring ambulation in mouse models of muscular dystrophy. J Vis Exp 2017;130:e56772–8.
49. Mathis DM, Furman JL, Norris CM. Preparation of acute hippocampal slices from rats and transgenic mice for the study of synaptic alterations during aging and amyloid pathology. J Vis Exp 2011;49:e2330–8.
50. Corona BT, Machingal MA, Criswell T, et al. Further development of a tissue engineered muscle repair construct in vitro for enhanced functional recovery following implantation in vivo in a murine model of volumetric muscle loss injury. Tissue Eng Part A 2012;18:1213–28. [PubMed: 22439962]
51. Minchew EC, Williamson NC, Readyoff AT, McClung JM, Spangenburg EE. Isometric skeletal muscle contractile properties in common strains of male laboratory mice. Front Physiol 2022;13:937132. [PubMed: 36267576]
52. Mendez J, Keys A. Density and composition of mammalian muscle. Metabol, Clin Exp 1960;9:184–8.
53. Brooks SV, Faulkner JA. Contractile properties of skeletal muscles from young, adult and aged mice. J Physiol 1988;404:71–82. [PubMed: 3253447]
54. Picard M, Ritchie D, Wright KJ, et al. Mitochondrial functional impairment with aging is exaggerated in isolated mitochondria compared to permeabilized myofibers. Aging Cell 2010;9:1032–46. [PubMed: 20849523]
55. Ryan TE, Schmidt CA, Green TD, Spangenburg EE, Neufer PD, McClung JM. Targeted expression of catalase to mitochondria protects against ischemic myopathy in high-fat diet-fed mice. Diabetes 2016;65:2553–68. [PubMed: 27284110]
56. Komlodi T, Sobotka O, Krumschnabel G, et al. Comparison of mitochondrial incubation media for measurement of respiration and hydrogen peroxide production. Methods Mol Biol 2018;1782:137–55. [PubMed: 29850998]
57. Li Puma LC, Hedges M, Heckman JM, et al. Experimental oxygen concentration influences rates of mitochondrial hydrogen peroxide release from cardiac and skeletal muscle preparations. Am J Physiol Regul Integr Compar Physiol 2020;318:R972–80.
58. Krumschnabel G, Fontana-Ayoub M, Sumbalova Z, et al. Simultaneous high-resolution measurement of mitochondrial respiration and hydrogen peroxide production. Methods Mol Biol 2015;1264:245–61. [PubMed: 25631019]
59. Janssen RC, Boyle KE. Microplate assays for spectrophotometric measurement of mitochondrial enzyme activity. Methods Mol Biol 2019;1978:355–68. [PubMed: 31119674]
60. Liu HM, Ferrington DA, Baumann CW, Thompson LV. Denervation-induced activation of the standard proteasome and immunoproteasome. PLoS One 2016;11:e0166831. [PubMed: 27875560]
61. Ferrington DA, Husom AD, Thompson LV. Altered proteasome structure, function, and oxidation in aged muscle. FASEB J 2005;19:644–6. [PubMed: 15677694]
62. Makris KI, Nella AA, Zhu Z, et al. Mitochondriopathy of peripheral arterial disease. Vascular 2007;15:336–43. [PubMed: 18053417]
63. Pipinos II, Judge AR, Zhu Z, et al. Mitochondrial defects and oxidative damage in patients with peripheral arterial disease. Free Radic Biol Med 2006;41:262–9. [PubMed: 16814106]
64. Fedorova M, Bollineni RC, Hoffmann R. Protein carbonylation as a major hallmark of oxidative damage: update of analytical strategies. Mass Spectrom Rev 2014;33:79–97. [PubMed: 23832618]
65. Powers SK, Morton AB, Ahn B, Smuder AJ. Redox control of skeletal muscle atrophy. Free Radic Biol Med 2016;98:208–17. [PubMed: 26912035]
66. Londhe P, Guttridge DC. Inflammation induced loss of skeletal muscle. Bone 2015;80:131–42. [PubMed: 26453502]
67. Costamagna D, Costelli P, Sampaolesi M, Penna F. Role of inflammation in muscle homeostasis and myogenesis. Mediators Inflamm 2015;2015:805172. [PubMed: 26508819]

68. Du J, Wang X, Miereles C, et al. Activation of caspase-3 is an initial step triggering accelerated muscle proteolysis in catabolic conditions. J Clin Invest 2004;113:115–23. [PubMed: 14702115]
69. Los M, Mozoluk M, Ferrari D, et al. Activation and caspase-mediated inhibition of PARP: a molecular switch between fibroblast necrosis and apoptosis in death receptor signaling. Mol Biol Cell 2002;13:978–88. [PubMed: 11907276]
70. Sanchez AM, Candau RB, Bernardi H. FoxO transcription factors: their roles in the maintenance of skeletal muscle homeostasis. Cell Mol Life Sci 2014;71:1657–71. [PubMed: 24232446]
71. Peris-Moreno D, Taillandier D, Polge C. MuRF1/TRIM63, master regulator of muscle mass. Int J Mol Sci 2020;21:6663–702. [PubMed: 32933049]
72. Milan G, Romanello V, Pescatore F, et al. Regulation of autophagy and the ubiquitin-proteasome system by the FoxO transcriptional network during muscle atrophy. Nat Commun 2015;6:6670. [PubMed: 25858807]
73. Xia Q, Huang X, Huang J, et al. The role of autophagy in skeletal muscle diseases. Front Physiol 2021;12:638983. [PubMed: 33841177]
74. Kapetanou M, Nespital T, Tain LS, Pahl A, Partridge L, Gonos ES. FoxO1 is a novel regulator of 20S proteasome subunits expression and activity. Front Cell Dev Biol 2021;9:625715. [PubMed: 33634126]
75. Loos B, du Toit A, Hofmeyr JH. Defining and measuring autophagosome flux-concept and reality. Autophagy 2014;10:2087–96. [PubMed: 25484088]
76. Pizzimenti M, Riou M, Charles AL, et al. The rise of mitochondria in peripheral arterial disease physiopathology: experimental and clinical data. J Clin Med 2019;8:2125–39. [PubMed: 31810355]
77. Lejay A, Meyer A, Schlagowski AI, et al. Mitochondria: mitochondrial participation in ischemia-reperfusion injury in skeletal muscle. Int J Biochem Cell Biol 2014;50:101–5. [PubMed: 24582887]
78. Gratl A, Wipper S, Frese JP, Raude B, Greiner A, Pesta D. The role of mitochondrial function in peripheral arterial disease: insights from translational studies. Int J Mol Sci 2021;22:8478–89. [PubMed: 34445191]
79. Fisher-Wellman KH, Neufer PD. Linking mitochondrial bioenergetics to insulin resistance via redox biology. Trends Endocrinol Metab 2012;23:142–53. [PubMed: 22305519]
80. Matsuda M, Shimomura I. Increased oxidative stress in obesity: implications for metabolic syndrome, diabetes, hypertension, dyslipidemia, atherosclerosis, and cancer. Obes Res Clin Pract 2013;7:e330–41. [PubMed: 24455761]
81. McMurray F, Patten DA, Harper ME. Reactive oxygen species and oxidative stress in obesity-recent findings and empirical approaches. Obesity (Silver Spring) 2016;24:2301–10. [PubMed: 27804267]
82. Espinosa A, Henriquez-Olguin C, Jaimovich E. Reactive oxygen species and calcium signals in skeletal muscle: a crosstalk involved in both normal signaling and disease. Cell Calcium 2016;60:172–9. [PubMed: 26965208]
83. Frohnert BI, Bernlohr DA. Protein carbonylation, mitochondrial dysfunction, and insulin resistance. Adv Nutr 2013;4:157–63. [PubMed: 23493532]
84. Rodriguez-Nuevo A, Diaz-Ramos A, Noguera E, et al. Mitochondrial DNA and TLR9 drive muscle inflammation upon opa1 deficiency. EMBO J 2018;37:e96553–71. [PubMed: 29632021]
85. Riley JS, Tait SW. Mitochondrial DNA in inflammation and immunity. EMBO Rep 2020;21:e49799. [PubMed: 32202065]
86. Shepard CR. TLR9 in MAFLD and NASH: at the intersection of inflammation and metabolism. Front Endocrinol (Lausanne) 2020;11:613639. [PubMed: 33584545]
87. Collins LV, Hajizadeh S, Holme E, Jonsson IM, Tarkowski A. Endogenously oxidized mitochondrial DNA induces in vivo and in vitro inflammatory responses. J Leukoc Biol 2004;75:995–1000. [PubMed: 14982943]
88. Kim J, Gupta R, Blanco LP, et al. VDAC oligomers form mitochondrial pores to release mtDNA fragments and promote lupus-like disease. Science 2019;366:1531–6. [PubMed: 31857488]
89. Tran TP, Tu H, Liu J, Muelleman RL, Li YL. Mitochondria-derived superoxide links to tourniquet-induced apoptosis in mouse skeletal muscle. PLoS One 2012;7:e43410. [PubMed: 22912870]

90. Bhat HK, Hiatt WR, Hoppel CL, Brass EP. Skeletal muscle mitochondrial DNA injury in patients with unilateral peripheral arterial disease. Circulation 1999;99:807–12. [PubMed: 9989967]
91. Gonzalez-Freire M, Moore AZ, Peterson CA, et al. Associations of peripheral artery disease with calf skeletal muscle mitochondrial DNA heteroplasmy. J Am Heart Assoc 2020;9:e015197. [PubMed: 32200714]
92. McDermott MM, Peterson CA, Sufit R, et al. Peripheral artery disease, calf skeletal muscle mitochondrial DNA copy number, and functional performance. Vasc Med 2018;23:340–8. [PubMed: 29734865]
93. Bayir H, Kagan VE. Bench-to-bedside review: Mitochondrial injury, oxidative stress and apoptosis−there is nothing more practical than a good theory. Crit Care 2008;12:206. [PubMed: 18341705]
94. Bloemberg D, Quadrilatero J. Autophagy, apoptosis, and mitochondria: molecular integration and physiological relevance in skeletal muscle. Am J Physiol Cell Physiol 2019;317:C111–30. [PubMed: 31017800]
95. Michelucci A, Liang C, Protasi F, Dirksen RT. Altered Ca(2+) handling and oxidative stress underlie mitochondrial damage and skeletal muscle dysfunction in aging and disease. Metabolites 2021;11:424–43. [PubMed: 34203260]
96. Espinosa A, Henríquez-Olguín C, Jaimovich E. Reactive oxygen species and calcium signals in skeletal muscle: a crosstalk involved in both normal signaling and disease. Cell Calcium 2016;60:172–9. [PubMed: 26965208]
97. Hyatt HW, Powers SK. The role of calpains in skeletal muscle remodeling with exercise and inactivity-induced atrophy. Int J Sports Med 2020;41:994–1008. [PubMed: 32679598]
98. Peterson CM, Johannsen DL, Ravussin E. Skeletal muscle mitochondria and aging: a review. J Aging Res 2012;2012:194821. [PubMed: 22888430]
99. Snel M, Jonker JT, Schoones J, et al. Ectopic fat and insulin resistance: pathophysiology and effect of diet and lifestyle interventions. Int J Endocrinol 2012;2012:983814. [PubMed: 22675355]
100. Meex RCR, Blaak EE, van Loon LJC. Lipotoxicity plays a key role in the development of both insulin resistance and muscle atrophy in patients with type 2 diabetes. Obes Rev 2019;20:1205–17. [PubMed: 31240819]
101. Inoguchi T, Li P, Umeda F, et al. High glucose level and free fatty acid stimulate reactive oxygen species production through protein kinase C−dependent activation of NAD(P)H oxidase in cultured vascular cells. Diabetes 2000;49:1939–45. [PubMed: 11078463]
102. Soldani C, Scovassi AI. Poly(ADP-ribose) polymerase-1 cleavage during apoptosis: an update. Apoptosis 2002;7:321–8. [PubMed: 12101391]
103. Mashimo M, Onishi M, Uno A, et al. The 89-kDa PARP1 cleavage fragment serves as a cytoplasmic PAR carrier to induce AIF-mediated apoptosis. J Biol Chem 2021;296:100046. [PubMed: 33168626]
104. Pacher P, Szabo C. Role of poly(ADP-ribose) polymerase 1 (PARP-1) in cardiovascular diseases: the therapeutic potential of PARP inhibitors. Cardiovasc Drug Rev 2007;25:235–60. [PubMed: 17919258]
105. Saini SK, Li L, Peek CB, et al. Associations of poly (ADP-Ribose) Polymerase1 abundance in calf skeletal muscle with walking performance in peripheral artery disease. Exp Gerontol 2020;140:111048. [PubMed: 32755612]
106. Chen G, Kroemer G, Kepp O. Mitophagy: an emerging role in aging and age-associated diseases. Front Cell Dev Biol 2020;8:200. [PubMed: 32274386]
107. Picca A, Wohlgemuth SE, McDermott MM, et al. Mitochondrial complex abundance, mitophagy proteins, and physical performance in people with and without peripheral artery disease. J Am Heart Assoc 2023;12:e027088. [PubMed: 36892048]
108. Karbowski M, Youle RJ. Regulating mitochondrial outer membrane proteins by ubiquitination and proteasomal degradation. Curr Opin Cell Biol 2011;23:476–82. [PubMed: 21705204]
109. Lavie J, De Belvalet H, Sonon S, et al. Ubiquitin-dependent degradation of mitochondrial proteins regulates energy metabolism. Cell Rep 2018;23:2852–63. [PubMed: 29874573]
110. Zhang M, Wang G, Peng T. Calpain-Mediated mitochondrial damage: an emerging mechanism contributing to cardiac disease. Cells 2021;10:2024–41. [PubMed: 34440793]

111. Chen Q, Thompson J, Hu Y, Dean J, Lesnefsky EJ. Inhibition of the ubiquitous calpains protects complex I activity and enables improved mitophagy in the heart following ischemia-reperfusion. Am J Physiol Cell Physiol 2019;317:C910–21. [PubMed: 31411917]

112. Ni R, Zheng D, Xiong S, et al. Mitochondrial Calpain-1 disrupts ATP synthase and induces superoxide generation in type 1 diabetic hearts: a novel mechanism contributing to diabetic cardiomyopathy. Diabetes 2016;65:255–68. [PubMed: 26470784]

113. Wilburn D, Ismaeel A, Machek S, Fletcher E, Koutakis P. Shared and distinct mechanisms of skeletal muscle atrophy: a narrative review. Ageing Res Rev 2021;71:101463. [PubMed: 34534682]

114. Koutakis P, Miserlis D, Myers SA, et al. Abnormal accumulation of desmin in gastrocnemius myofibers of patients with peripheral artery disease: associations with altered myofiber morphology and density, mitochondrial dysfunction and impaired limb function. J Histochem Cytochem 2015;63:256–69. [PubMed: 25575565]

115. Ismaeel A, Miserlis D, Papoutsi E, et al. Endothelial cell-derived pro-fibrotic factors increase TGF-beta1 expression by smooth muscle cells in response to cycles of hypoxia-hyperoxia. Biochim Biophys Acta Mol Basis Dis 2022;1868:166278. [PubMed: 34601016]

116. Valle-Tenney R, Rebolledo DL, Lipson KE, Brandan E. Role of hypoxia in skeletal muscle fibrosis: synergism between hypoxia and TGF-beta signaling upregulates CCN2/CTGF expression specifically in muscle fibers. Matrix Biol 2020;87:48–65. [PubMed: 31669521]

117. Rebolledo DL, Lipson KE, Brandan E. Driving fibrosis in neuromuscular diseases: role and regulation of connective tissue growth factor (CCN2/CTGF). Matrix Biol Plus 2021;11:100059. [PubMed: 34435178]

118. Tu H, Qian J, Zhang D, et al. Different responses of skeletal muscles to femoral artery ligation-induced ischemia identified in BABL/c and C57BL/6 mice. Front Physiol 2022;13:1014744. [PubMed: 36187770]

119. Pabon M, Cheng S, Altin SE, et al. Sex differences in peripheral artery disease. Circ Res 2022;130:496–511. [PubMed: 35175843]

AT A GLANCE COMMENTARY

Panagiotis Koutakis et al.

Background

Peripheral artery disease (PAD) causes ischemic myopathy which escalates patient morbidity and mortality. Current pathophysiologic knowledge largely stems from acute hindlimb ischemia (HLI) studies using young, healthy rodents, with limited translatability to humans. With our high-fat aged mouse model, we demonstrate the combined negative impact of age and obesity - major PAD risk factors, on muscle structure and function.

Translational Significance

Chronic HLI induced a myopathy in aged mice, which was exacerbated by obesity and showed features consistent with moderate-stage human PAD. Our model's resemblance to PAD could prove invaluable for evaluating new therapeutics for translation to clinical practice.

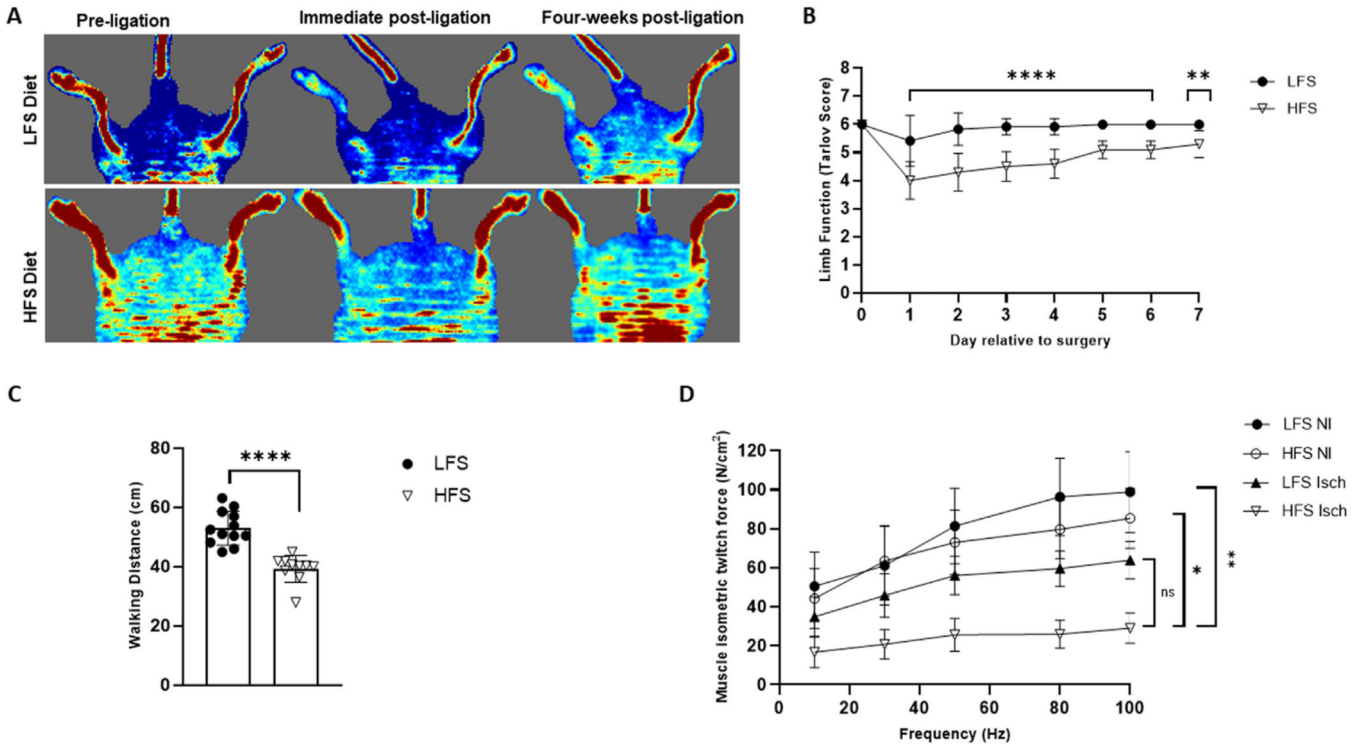

Fig 1.

Postoperative doppler imaging, limb function score, ambulatory ability, and *ex vivo* muscle contractility. (A) Representative pre- and immediate postligation doppler images confirming blood flow (depicted as red on the image) was reduced distal to the ligatures of the affected (left) limb in low-fat, low-sucrose (LFS)-fed and high-fat, high-sucrose (HFS)-fed mice. Representative doppler images showing change in blood flow to the affected limb 4-weeks following ligation are also provided. (B) A mixed effect ANOVA and pairwise comparisons using Bonferroni adjustment revealed reduced Tarlov scores (i.e., functional deficits) in mice fed a HFS diet ($n = 10$) but were unaltered in LFS-fed mice ($n = 12$). Tarlov scores are defined as: no movement (0), barely visible movement, nonweight bearing (1), frequent and vigorous movement but nonweight bearing (2), supports weight and may take 1 or 2 steps (3), walks with a mild deficit (4), normal but slow walking (5), full and fast walking (6).[32,44] (C) An independent samples t-test showed 4-week postoperative 6-minute walking distance was reduced in obese mice compared to their LFS-fed counterparts. (D) Peak isometric force (measured at 100 Hz) was reduced in isolated ischemic (Isch) soleus muscles from both HFS and LFS-fed mice compared to non-ischemic (NI) muscle from the contralateral limb. Two-way ANOVA with Tukey post-hoc tests used for analysis. Data are displayed as mean ± SE; ns represents no significant difference, * $P < 0.05$, ** $P < 0.01$, **** $P < 0.0001$.

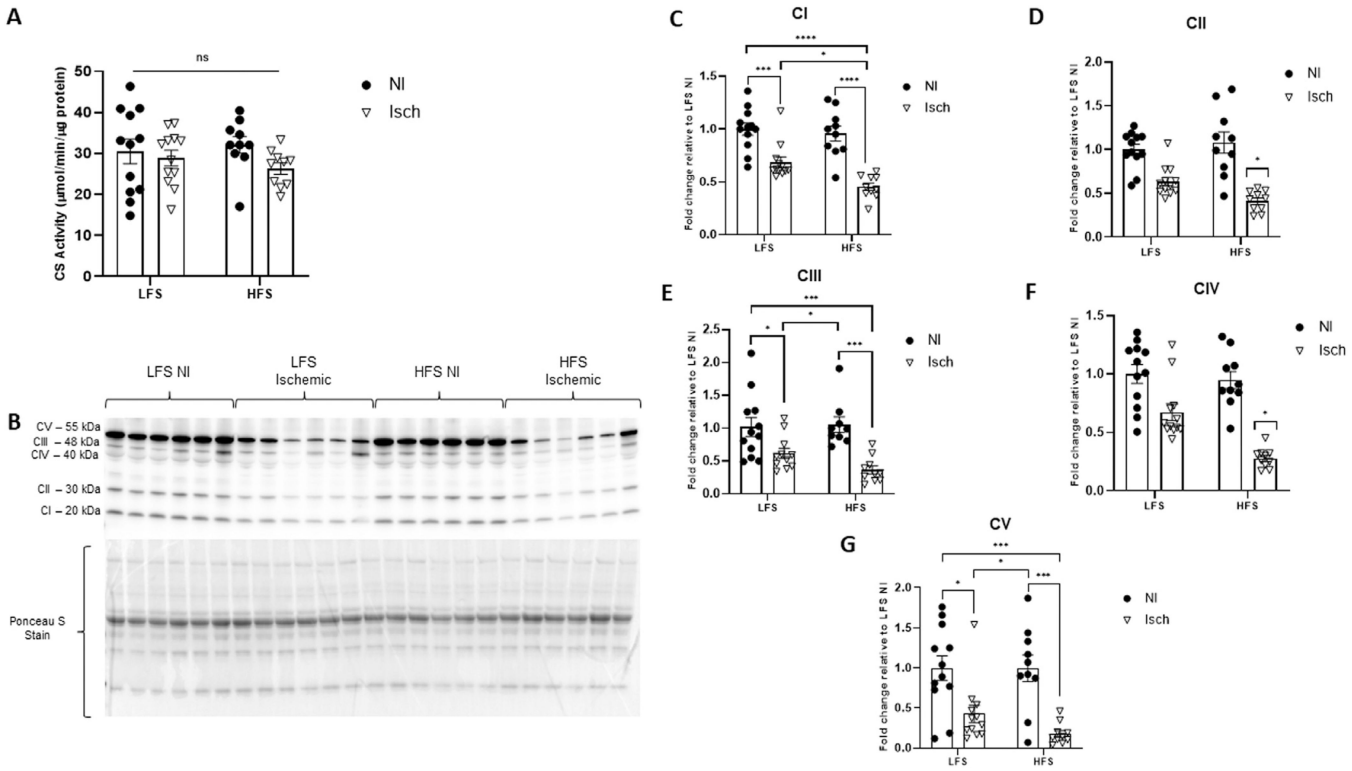

Fig 2.

The impact of chronic hindlimb ischemia on intramuscular mitochondrial content varies based on animal obesity status. (A) Overall mitochondrial content assessed via citrate synthase (CS) activity. (B) Representative western blot of the individual mitochondrial electron transport chain complexes I − V in ischemic (Isch) and nonischemic (NI) quadricep muscle from mice fed a high-fat, high sucrose (HFS) or low-fat, low-sucrose (LFS) diet. Ponceau S staining represents total protein per lane used for normalization. Fold change of (C) Complex I (CI), (D) Complex II (CII), (E) Complex III (CIII), (F) Complex IV (CIV) and (G) Complex V (CV) protein expression relative to NI muscle from LFS-fed control mice. Two-way ANOVA with Tukey post-hoc tests used for analyzes. Data are mean ± SE; ns represents no significant difference, * $P < 0.05$, *** $P < 0.001$, **** $P < 0.0001$ (n = 10−12 mice per group).

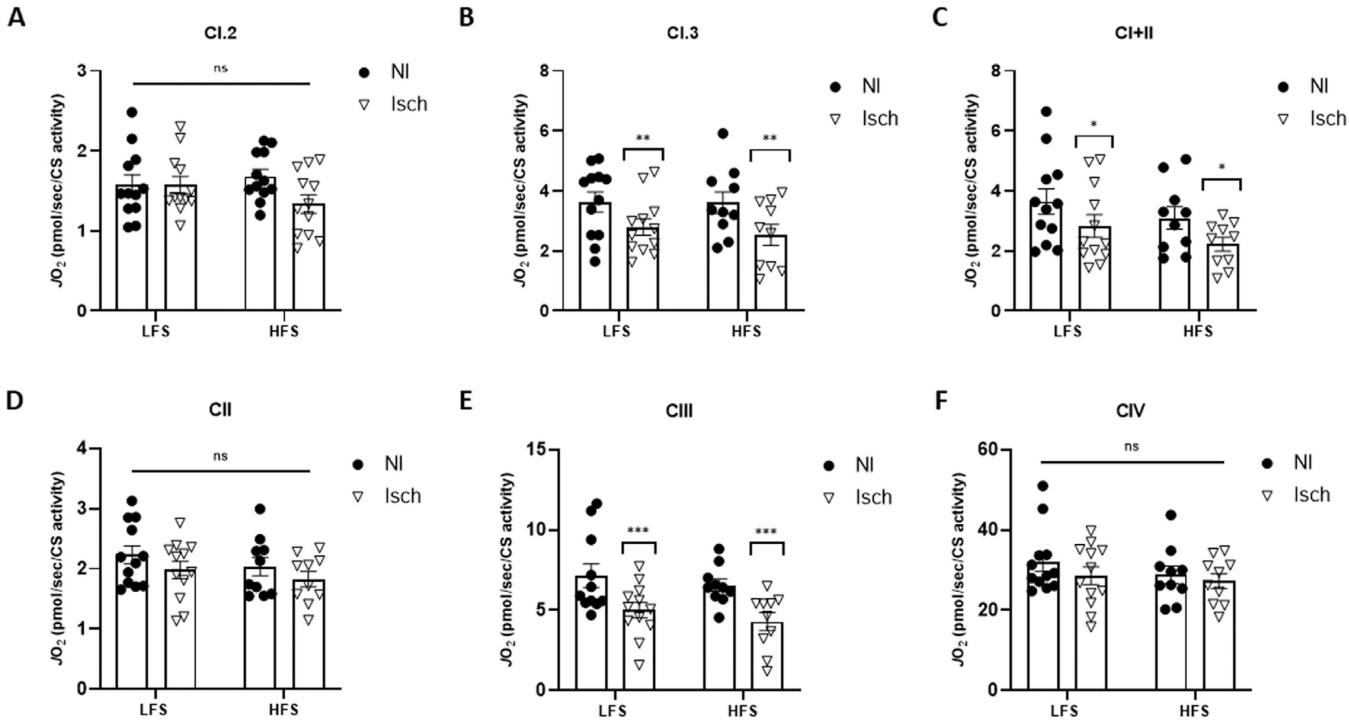

Fig 3.

Mitochondrial respiration is reduced in ischemic muscle of mice with and without obesity. Oxygen consumption rate (JO_2) in permeabilized ischemic (Isch) and nonischemic (NI) gastrocnemius muscle fibers from mice fed a low-fat, low-sucrose (LFS) ($n = 12$) and high-fat, high-sucrose (HFS) ($n = 10$) diet. JO_2 measured during (A) Complex I, state 2 respiration (CI.2), (B) Complex I, state 3 respiration (CI.3), (C) combined Complex I and II respiration (CI+II), (D) Complex II respiration (CII), (E) Complex III respiration and (F) Complex IV respiration (CIV). Two-way ANOVA with Tukey post-hoc tests used for analyzes. Data are mean ± SE; ns represents no significant difference between groups, * $P < 0.05$, ** $P < 0.01$, *** $P < 0.001$.

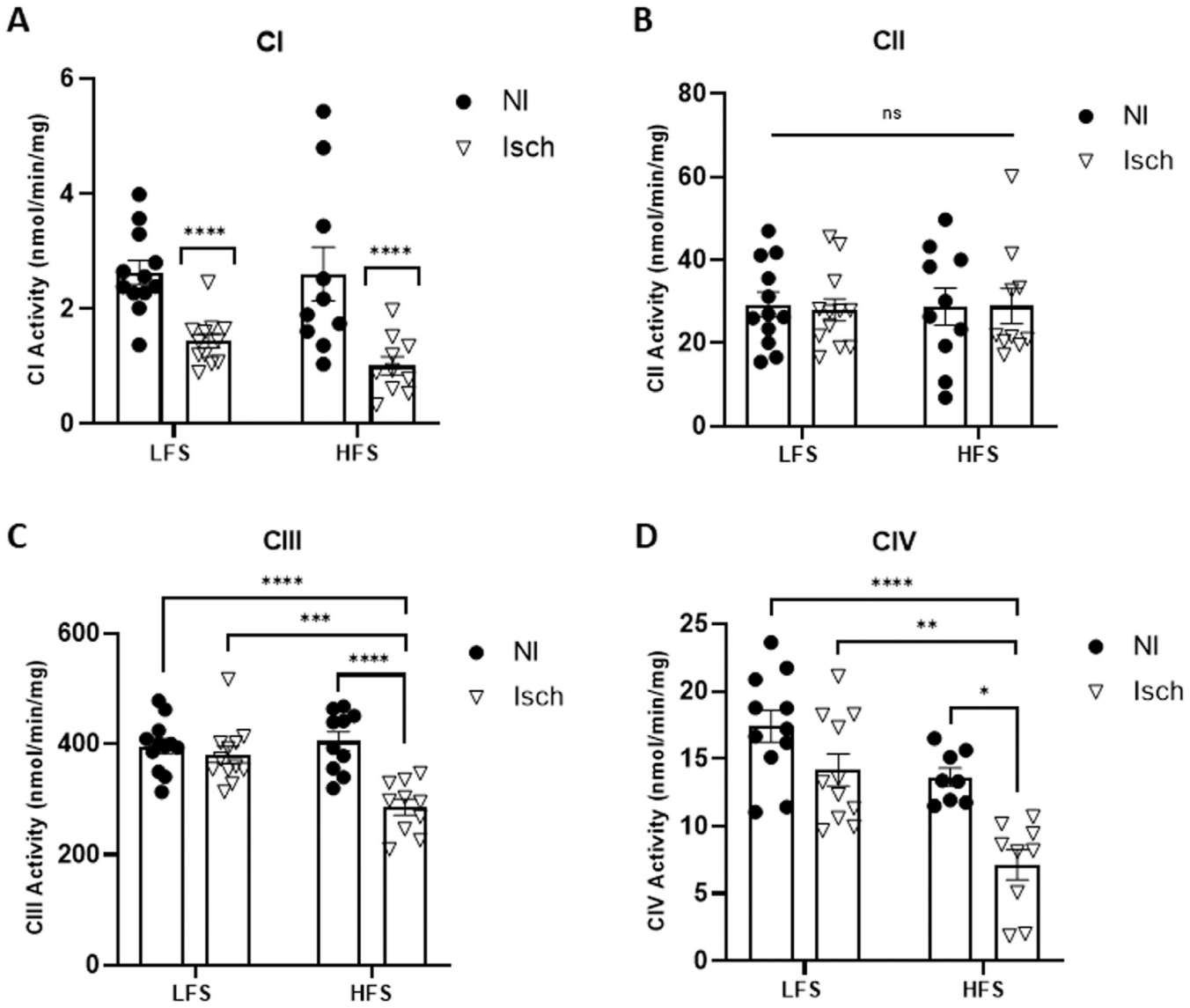

Fig 4.

Mitochondrial enzymatic activity is differentially impacted by chronic ischemia based on animal diet.

Enzymatic activity of electron transport chain (A) Complex I (CI), (B) Complex II (CII), (C) Complex III and (D) Complex IV measured in ischemic (Isch) and nonischemic (NI) quadricep muscle lysates from mice fed a low-fat, low-sucrose (LFS) and high-fat, high-sucrose (HFS) diet. Two-way ANOVA with Tukey post-hoc tests used for analyzes. Data are mean ± SE; ns represents no significant difference between groups, * $P < 0.05$, ** $P < 0.01$, *** $P < 0.001$, **** $P < 0.0001$ ($n = 8-12$ samples per group).

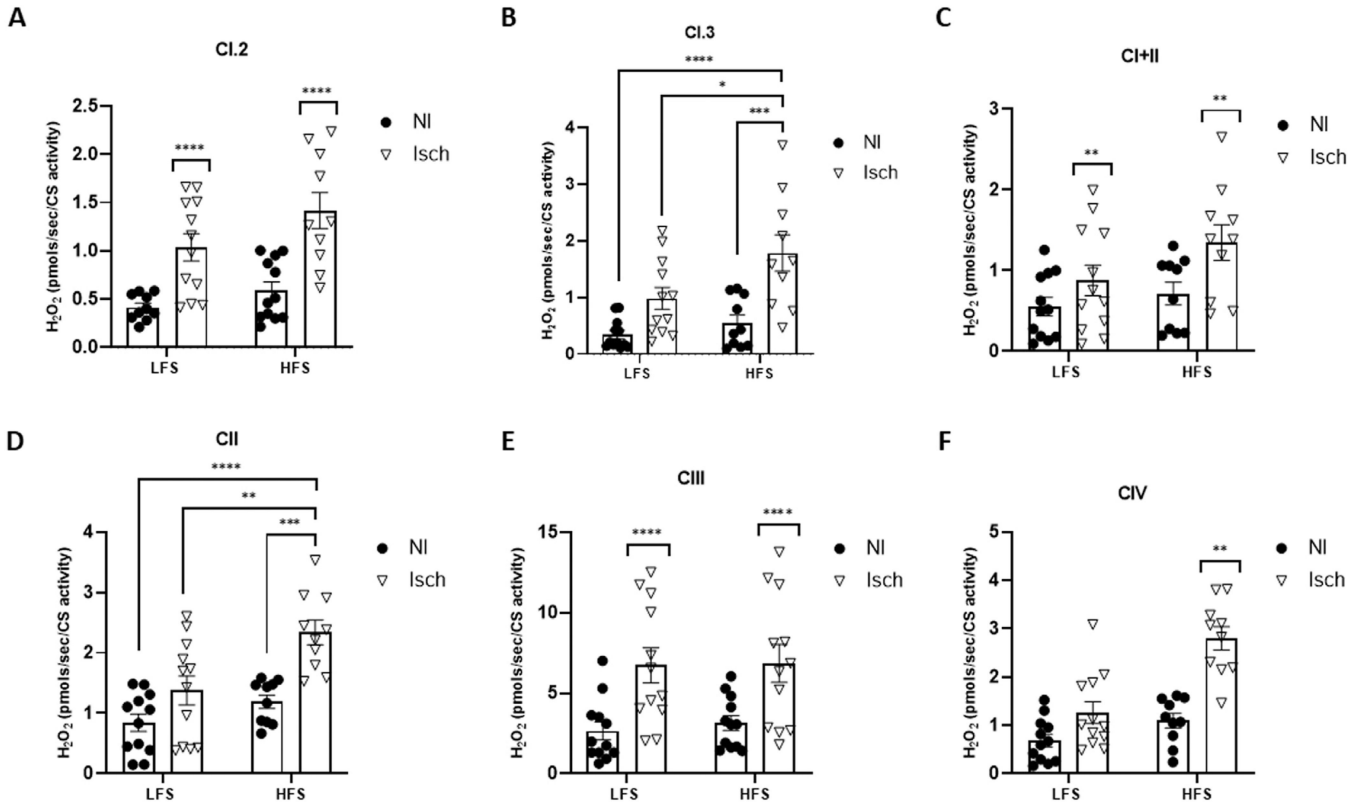

Fig 5.

Mitochondrial H_2O_2 emission is increased in ischemic muscle and varies by animal obesity status.

The rate of hydrogen peroxide (H_2O_2) produced in permeabilized ischemic (Isch) and nonischemic (NI) gastrocnemius muscle fibers from mice fed a low-fat, low-sucrose (LFS) ($n = 12$) and high-fat, high-sucrose (HFS) ($n = 10$) diet. H_2O_2 emitted during (A) Complex I, state 2 respiration (CI.2), (B) Complex I, state 3 respiration (CI.3), (C) combined Complex I and II respiration (CI+II), (D) Complex II respiration (CII), (E) Complex III respiration and (F) Complex IV respiration (CIV). Two-way ANOVA with Tukey post-hoc tests used for analyzes. Data are mean ± SE; asterixis denote * $P < 0.05$, ** $P < 0.01$, *** $P < 0.001$, **** $P < 0.0001$.

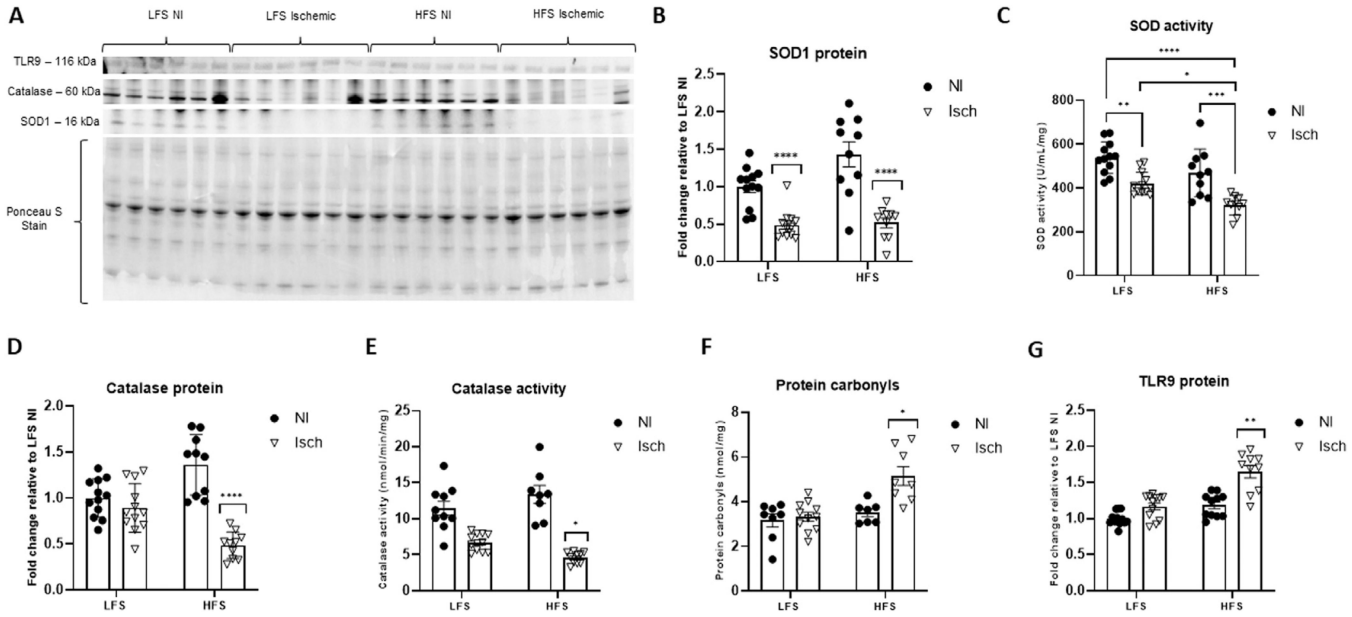

Fig 6.

The severity of ischemia-induced intramuscular oxidative stress and inflammation is increased with obesity. (A) Representative western blot of superoxide dismutase-1 (SOD1), catalase and toll-like receptor 9 (TLR9) protein in ischemic (Isch) and nonischemic (NI) muscle from mice fed a high-fat, high sucrose (HFS) or low-fat, low-sucrose (LFS) diet. Ponceau S staining represents total protein per lane used for normalization. (B) Fold change of SOD1 protein expression, (C) SOD enzymatic activity, (D) fold change of catalase protein expression, (E) catalase activity, (F) intramuscular protein carbonyl accumulation (G) fold change in TLR9 protein content. Two-way ANOVA with Tukey post-hoc tests used for analyzes. Data are mean ± SE; * represents $P < 0.05$, ** $P < 0.01$, *** $P < 0.001$, **** $P < 0.0001$ ($n = 8-12$ samples per group).

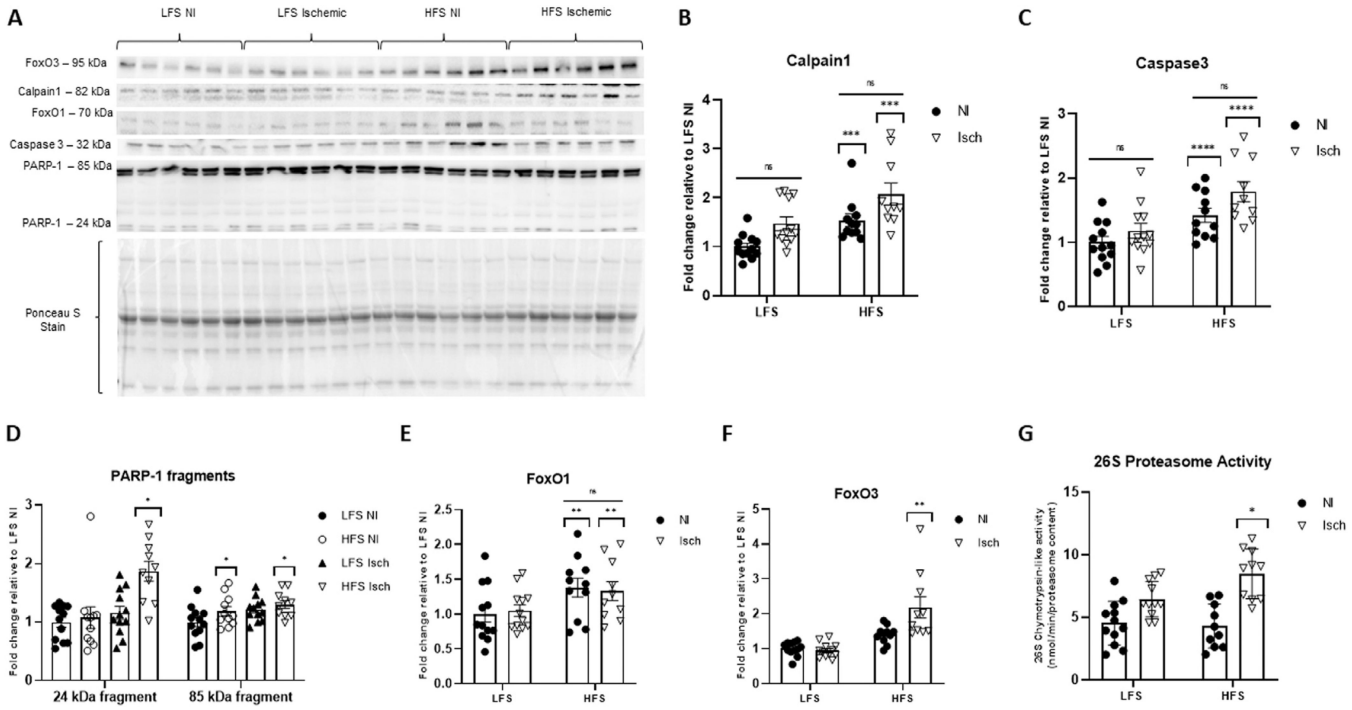

Fig 7.

Muscle protein breakdown varies in obese and nonobese mice with chronic hindlimb ischemia.

(A) Representative western blot showing calpain1, caspase 3, poly (ADP-ribose) polymerase 1 (PARP-1) fragments (at 24 kDa and 85 kDa molecular weights), forkhead box O1 (FoxO1), and forkhead box O3 (FoxO3) in ischemic (Isch) and nonischemic (NI) gastrocnemius muscle from mice fed a high-fat, high sucrose (HFS) or low-fat, low-sucrose (LFS) diet. Ponceau S staining represents total protein per lane used for normalization. Fold change of (B) calpain1, (C) caspase 3, (D) PARP-1 fragments, (E) FoxO1 and (F) FoxO3 protein expression relative to NI muscle from LFS-fed control mice. (G) Chymotrypsin-like activity of the 26S proteasome. Two-way ANOVA with Tukey post-hoc tests used for analyzes. Data are mean ± SE; ns represents no significant difference between groups, * $P < 0.05$, ** $P < 0.01$, *** $P < 0.001$, **** $P < 0.0001$ ($n = 10-12$ samples per group).

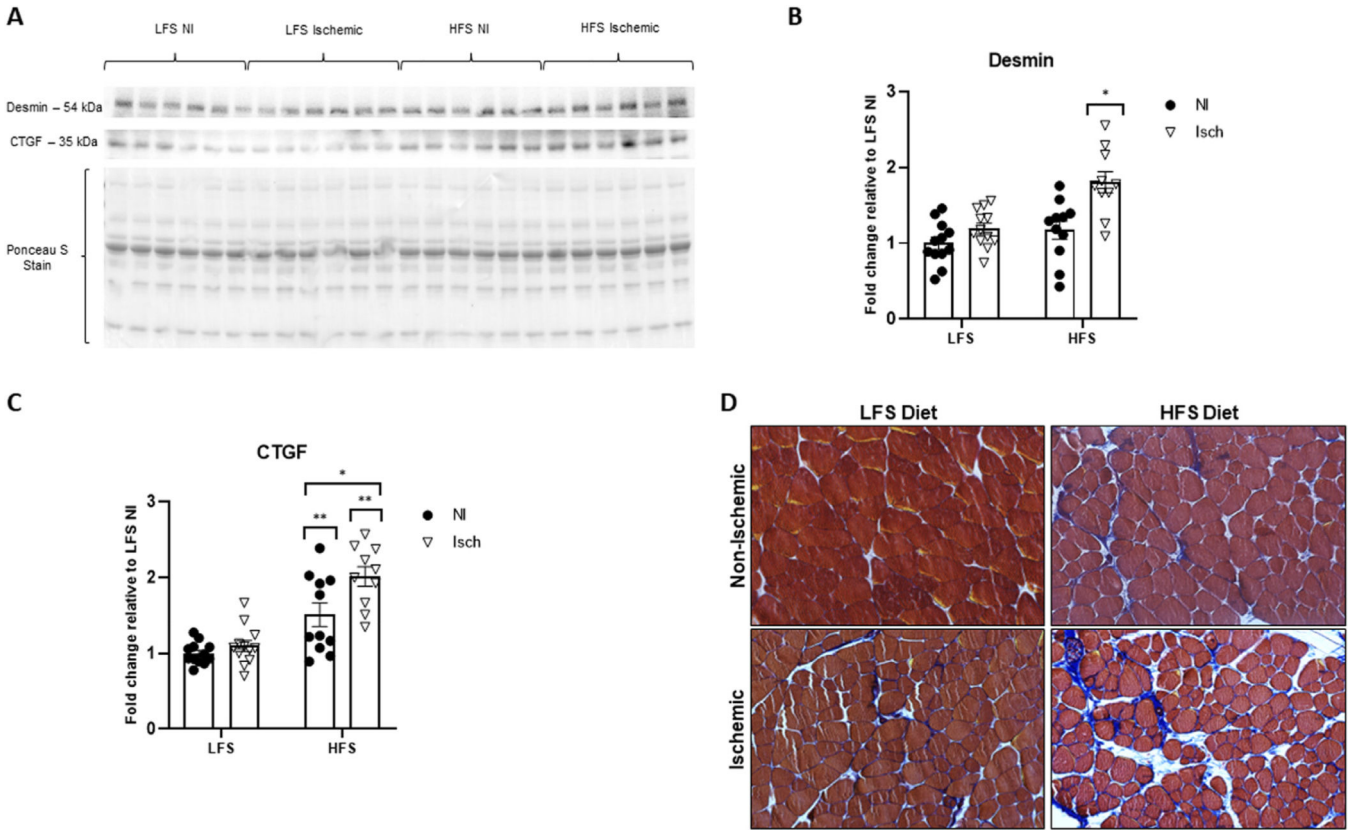

Fig 8.

Obesity promotes chronic ischemia-induced cytoskeletal damage and muscle fibrosis. (A) Representative western blot showing the cytoskeletal protein desmin, as well as the pro-fibrotic connective tissue growth factor (CTGF) band intensity in ischemic (Isch) and nonischemic (NI) gastrocnemius muscle from mice fed a high-fat, high sucrose (HFS) or low-fat, low-sucrose (LFS) diet. Ponceau S staining represents total protein per lane used for normalization. Fold change of (B) desmin and (C) CTGF protein expression relative to NI muscle from LFS-fed control mice. Two-way ANOVA with Tukey post-hoc tests used for analyzes. Data are mean ± SE; * represents $P < 0.05$, ** $P < 0.01$ ($n = 10-12$ samples per group). (D) Representative image of Masson-trichrome stained adductor muscle sections captured under bright-filed conditions (sarcoplasm, red; fibrous connective tissue, blue). There is an obvious increase in connective tissue deposition in the ischemic muscle of chronically obese mice.

Table 1

Gene expression of muscle proteolytic markers

mRNA target	LFS nonischemic (control) muscle	LFS ischemic muscle	HFS nonischemic muscle	HFS ischemic muscle
Calpain1	1.00 ± 0.27	1.41 ± 0.45 (0.3211)	1.23 ± 0.28 (0.8991)	0.93 ± 0.29 (0.6851)
Caspase 3	1.00 ± 0.30	0.65 ± 0.73 (0.2385)	1.01 ± 0.36 (0.1774)	1.99 ± 0.87 (0.1902)
FoxO1	1.00 ± 0.31	1.09 ± 0.31 (0.2922)	1.25 ± 0.50 (0.4171)	1.02 ± 0.87 (0.6001)
FoxO3	1.00 ± 0.22	1.92 ± 0.44 (0.3211)	1.32 ± 0.40 (0.2887)	1.09 ± 0.36 (0.5212)
Fbxo32	1.00 ± 0.46	1.33 ± 0.42 (0.3524)	1.40 ± 0.56 (0.7546)	1.33 ± 0.65 (0.8537)
TRIM63	1.00 ± 0.38	1.70 ± 0.43 (0.3254)	1.19 ± 0.45 (0.6783)	1.03 ± 0.36 (0.4890)
PSMB5	1.00 ± 0.15	1.54 ± 0.31 (0.1829)	0.71 ± 0.15 (0.1036)	0.83 ± 0.23 (0.5223)
Atg 7	1.00 ± 0.16	1.37 ± 0.36 (0.1830)	0.76 ± 0.13 (0.1101)	1.15 ± 0.27 (0.5574)
Atg 10	1.00 ± 0.23	1.00 ± 0.30 (0.1706)	0.92 ± 0.22 (0.8099)	1.06 ± 0.33 (0.8701)
Atg 12	1.00 ± 0.20	1.20 ± 0.25 (0.2271)	0.89 ± 0.16 (0.4064)	0.91 ± 0.25 (0.5369)
LC3 alpha	1.00 ± 0.22	1.39 ± 0.37 (0.3127)	0.88 ± 0.22 (0.7604)	0.98 ± 0.28 (0.7190)
p62	1.00 ± 0.27	1.12 ± 0.49 (0.2919)	0.97 ± 0.25 (0.6977)	0.88 ± 0.30 (0.5433)

Note: Values are mean fold up- or down-regulation vs control LFS nonischemic muscle ± SE with *P*-value versus control in parentheses ($n = 12$ and $n = 10$ in low-fat, low-sucrose (LFS) and high-fat, high sucrose (HFS) diet groups, respectively).